

Position distribution in a generalised run and tumble process

David S. Dean

Univ. Bordeaux and CNRS, Laboratoire Ondes et Matière d'Aquitaine (LOMA), UMR 5798, F-33400 Talence, France

Satya N. Majumdar

LPTMS, CNRS, Univ. Paris-Sud, Université Paris-Saclay, 91405 Orsay, France

Hendrik Schawe

LPTM, UMR 8089, CY Cergy Paris Université, CNRS, 95000 Cergy, France

We study a class of stochastic processes of the type $\frac{d^n x}{dt^n} = v_0 \sigma(t)$ where $n > 0$ is a positive integer and $\sigma(t) = \pm 1$ represents an ‘active’ telegraphic noise that flips from one state to the other with a constant rate γ . For $n = 1$, it reduces to the standard run and tumble process for active particles in one dimension. This process can be analytically continued to any $n > 0$ including non-integer values. We compute exactly the mean squared displacement at time t for all $n > 0$ and show that at late times while it grows as $\sim t^{2n-1}$ for $n > 1/2$, it approaches a constant for $n < 1/2$. In the marginal case $n = 1/2$, it grows very slowly with time as $\sim \ln t$. Thus the process undergoes a *localisation* transition at $n = 1/2$. We also show that the position distribution $p_n(x, t)$ remains time-dependent even at late times for $n \geq 1/2$, but approaches a stationary time-independent form for $n < 1/2$. The tails of the position distribution at late times exhibit a large deviation form, $p_n(x, t) \sim \exp\left[-\gamma t \Phi_n\left(\frac{x}{x^*(t)}\right)\right]$, where $x^*(t) = v_0 t^n / \Gamma(n + 1)$. We compute the rate function $\Phi_n(z)$ analytically for all $n > 0$ and also numerically using importance sampling methods, finding excellent agreement between them. For three special values $n = 1$, $n = 2$ and $n = 1/2$ we compute the exact cumulant generating function of the position distribution at all times t .

I. INTRODUCTION

The position of an overdamped Brownian particle in one dimension evolves with time via the stochastic Langevin equation

$$\frac{dx}{dt} = \sqrt{2D} \eta(t), \quad (1)$$

where the friction coefficient is set to unity, D represents the diffusion constant and $\eta(t)$ is a zero mean Gaussian white noise with correlator $\langle \eta(t)\eta(t') \rangle = \delta(t - t')$. A natural generalisation of this process is a family of stochastic processes indexed by a positive integer n [1]

$$\frac{d^n x}{dt^n} = \sqrt{2D} \eta(t), \quad (2)$$

that reduces to the Brownian motion for $n = 1$. For any $n > 1$, the process $x(t)$, though simply Gaussian, is non-Markovian [1, 2] due to the higher order derivative in (2).

For $n = 2$, (2) represents the celebrated random acceleration process introduced by Wang and Uhlenbeck [3], where an undamped particle is subjected to a random force modelled by the white noise. This problem arises quite naturally in dispersion theory. Consider a particle in a plane where its y -component undergoes a Brownian motion $dy/dt = \eta(t)$, while in the x -direction it gets convected by a noiseless flow velocity field $u(y(t))$ that depends only on the y -coordinate at time t , $dx/dt = u(y(t))$. Thus, for a shear flow such that $u(y) = \gamma y$ (with γ representing the shear rate), the x -component undergoes the random acceleration process: $d^2x/dt^2 = \gamma \eta(t)$. In the mathematics literature, the process $x(t)$ in (2) with $n = 2$ has also been studied extensively [4], as it represents the area under a Brownian curve $x(t) = \int_0^t B(\tau) d\tau$ (where $B(t)$ represents a Brownian motion). The random acceleration problem also has applications in the context of granular collapse [5].

For general n , an interesting application of (2) can be found in the study of height fluctuations in equilibrium interface models [6]. Here one considers the height profile $h(\mathbf{x}, t)$ of an interface on a d -dimensional substrate of finite size, with \mathbf{x} denoting a point on the substrate. At long times, the system reaches a stationary state where the height profile, as a function of the spatial distance along a fixed direction on the substrate, can be effectively described by the process (2) (with t denoting the spatial distance and x representing the height of the interface), where the exponent n can be expressed in terms of the dynamical exponent of the interface [2, 6]. Path integrals related to (2) with $n > 1$ also arise in the treatment of semi-flexible polymers incorporating bending as well as elastic energy [7–12], in higher derivative field theories describing diblock copolymer phase separation [13, 14], and also in relativistic quantum mechanics [15].

The process (2) can be represented (assuming for simplicity that all $(n - 1)$ derivatives vanish at $t = 0$) [1]

$$x(t) = \frac{\sqrt{2D}}{\Gamma(n)} \int_0^t ds (t - s)^{n-1} \eta(s) \quad (3)$$

which reduces to (2) by repeated differentiation. Using this representation, one can then analytically continue the process even to non-integer (fractional) $n > 0$. Note that since $x(t)$ is a linear combination of Gaussian white noises, it is clear that $x(t)$ is also a Gaussian process at all times t , with zero mean and a variance that can be trivially computed from (3) using the delta correlation of the noise $\langle \eta(t)\eta(t') \rangle = \delta(t - t')$. One gets

$$\sigma_n^2(t) = \langle x^2(t) \rangle = \frac{2D t^{2n-1}}{(2n-1)\Gamma^2(n)}. \quad (4)$$

Thus the position distribution, at any fixed time t , is given by a purely Gaussian distribution

$$p_n(x, t) = \sqrt{\frac{(2n-1)\Gamma^2(n)}{4\pi D t^{2n-1}}} \exp\left[-\frac{(2n-1)\Gamma^2(n)}{4D t^{2n-1}} x^2\right] \quad (5)$$

valid for all x , all t and all $n > 1/2$. Note that for $0 < n < 1/2$, the process (3) is not well defined, because at short times, the particle gets an infinitely large kick by the noise which sends it to $\pm\infty$ leading to a pathological situation.

Finally, let us remark that even though the position distribution for the process (3) is trivially Gaussian at all times for all $n > 1/2$, the first-passage properties of the process for any $n \neq 1$ is highly nontrivial due to non-Markovian nature of the process [1, 2]. Even for $n = 2$, it took almost 47 years, since the original introduction of the problem by Wang and Uhlenbeck in 1945, to compute the first-passage probability [8, 16, 17]. The first-passage properties for

general $n > 1/2$ have been studied extensively in recent times by various methods and are again nontrivial due to non-Markovian nature of the process for $n \neq 1$ [1, 2, 18–20].

Another non-Markovian generalisation of the ordinary Brownian motion in (1) that has been studied extensively is the so called ‘persistent Brownian motion’ [21–24]

$$\frac{dx}{dt} = v_0 \sigma(t), \quad (6)$$

where v_0 denotes the intrinsic speed of a particle and the noise $\sigma(t)$ is telegraphic: it can take two values ± 1 . It flips from one value to the other with a finite rate γ . This model has seen a recent resurgence of interest in the context of ‘run and tumble’ (RTP) dynamics of an active particle like the E. Coli bacteria [25, 26]. In one dimension, when the noise $\sigma(t)$ remains unflipped for a certain duration, the particle ‘runs’ with speed v_0 in that direction. When $\sigma(t)$ changes sign, it represents a ‘tumble’ and the particle changes its direction of motion and goes for another run and so on.

The effective driving noise $\xi(t) = v_0 \sigma(t)$ in (6) is ‘coloured’ since its autocorrelation function (see Section IV for a simple derivation)

$$\langle \xi(t)\xi(t') \rangle = v_0^2 e^{-2\gamma|t-t'|}. \quad (7)$$

has a finite persistence time $\sim \gamma^{-1}$. The noise thus has a memory of finite duration which makes the process $x(t)$ non-Markovian. In the limit $\gamma \rightarrow \infty$, $v_0 \rightarrow \infty$ but keeping the ratio $D = v_0^2/2\gamma$ fixed, the noise $\xi(t)$ reduces to a white noise since

$$\langle \xi(t)\xi(t') \rangle = \frac{v_0^2}{\gamma} \left[\gamma e^{-2\gamma|t-t'|} \right] \rightarrow 2D \delta(t-t'). \quad (8)$$

Thus the RTP dynamics (6) reduces to an ordinary Brownian motion in this diffusive limit.

Several properties of the one dimensional RTP process (6) such as the position distribution [23, 27–33] and first-passage properties [30, 31, 34–40] are well known. For example, for a particle starting from $x = 0$ at $t = 0$ with $\sigma(0) = \pm 1$ with equal probability, the position distribution $p_1(x, t)$ at finite t is highly nontrivial. The distribution is supported over the interval $x \in [-v_0 t, v_0 t]$ and is given for $|x| \leq v_0 t$ by

$$p_1(x, t) = \frac{e^{-\gamma t}}{2} \left\{ \delta(x - v_0 t) + \delta(x + v_0 t) + \frac{\gamma}{2v_0} \left[I_0(\rho) + \frac{\gamma I_1(\rho)}{\rho} \right] \theta(v_0 t - |x|) \right\}; \quad \text{where } \rho = \sqrt{v_0^2 t^2 - x^2} \frac{\gamma}{v_0} \quad (9)$$

and $I_0(\rho)$ and $I_1(\rho)$ are modified Bessel functions of the first kind. The edges of the support $x = \pm v_0 t$ corresponds to the maximal possible displacements of the particle on either sides of the origin (corresponding to the event when the noise $\sigma(t)$ does not flip sign at all during time t). As time progresses, the centres of the two delta functions at the two edges move ballistically away with speed $\pm v_0$ (representing two *light cones*), but their amplitudes decay exponentially with time t since the probability that $\sigma(t)$ retains its sign up to t decays as $\sim e^{-\gamma t}$. In the central part near $x = 0$, the distribution $p_1(x, t)$ approaches a Gaussian form at late times, as one would expect since the RTP at late times does reduce to the ordinary Brownian motion. These features of $p_1(x, t)$ are well captured by a large deviation form exhibited by the distribution. To see this, consider the limit $t \rightarrow \infty$, $|x| \rightarrow \infty$ but with the ratio $z = x/v_0 t$ fixed. Using the asymptotic behavior $I_m(\rho) \sim e^\rho / \sqrt{2\pi\rho}$ as $\rho \rightarrow \infty$ for any $m > 0$, one finds that $p_1(x, t)$ in (9) exhibits the following large deviation form

$$p_1(x, t) \sim \exp \left[-\gamma t \Phi_1 \left(\frac{x}{v_0 t} \right) \right] \quad \text{with } \Phi_1(z) = 1 - \sqrt{1 - z^2}, \quad -1 \leq z \leq 1. \quad (10)$$

The rate function behaves quadratically $\Phi_1(z) \approx z^2/2$ as $z \rightarrow 0$. Substituting this behaviour in (10), one finds that for $|x| \ll v_0 t$, the distribution converges to the Gaussian form, $p_1(x, t) \sim \exp[-x^2/4Dt]$, with $D = v_0^2/2\gamma$, as expected for a Brownian motion with diffusion constant D . Thus the large deviation regime valid at the tails, when extrapolated towards the peak, matches smoothly with the inner Gaussian peak characterizing the typical fluctuations around the mean.

Given that a finite memory encoded in the driving telegraphic noise induces a nontrivial position distribution $p_1(x, t)$ at finite t for the RTP process (6), it is natural to investigate the similar question for the generalised RTP process that we introduce here

$$\frac{d^n x}{dt^n} = v_0 \sigma(t), \quad (11)$$

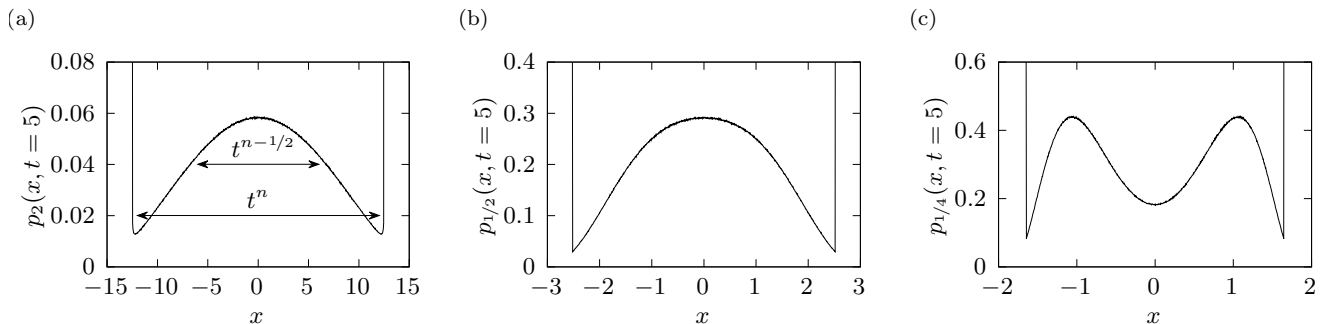


FIG. 1. The position distribution $p_n(x, t)$ vs. x for a fixed $t = 5$ obtained from simulations for three different values of n : (a) $n = 2$ (b) $n = 1/2$ and (c) $n = 1/4$. In all cases, the distribution has a support on $x \in [-x^*(t), x^*(t)]$ where $x^*(t) = v_0 t^n / \Gamma(n + 1)$. In (a), where $n > 1/2$, the typical fluctuations grow as $\sim t^{n-1/2}$ at late times and the distribution on this scale approaches a Gaussian form (near the peak). In (c), where $n < 1/2$, the typical fluctuations are of $O(1)$ at late times and the distribution approaches a time-independent double-humped structure at late times. The case (b) where $n = 1/2$ is the marginal case, separating the ‘localised’ phase ($n < 1/2$) and the ‘de-localised’ phase ($n > 1/2$), where the typical fluctuations grow logarithmically at late times and the distribution remains time-dependent for large t . In all the three cases, the distribution on the large deviation scale, when $x \sim x^*(t)$, satisfies the large deviation form in (13).

where $n > 0$ is a positive integer and $\sigma(t) = \pm 1$ is the dichotomous telegraphic noise. For $n = 1$, this process reduces to the standard RTP (6). For general n , this is an ‘active’ counterpart of the ‘passive’ white noise driven process (2). The activeness arises from the driving noise being ‘coloured’, i.e., with a finite memory encoded in the persistence time γ^{-1} . Once again, we can use the integral representation

$$x(t) = \frac{v_0}{\Gamma(n)} \int_0^t ds (t-s)^{n-1} \sigma(s) \quad (12)$$

to define the process for any $n > 0$, including non-integer values. In this paper, our main goal is to simply study the position distribution $p_n(x, t)$ of the process (12) for general $n > 0$.

Let us highlight briefly our main results. First, we show that the distribution $p_n(x, t)$ of the process (12) is well defined for any $n > 0$, unlike the white noise driven process (3) which is pathological for $0 < n < 1/2$. Secondly, we find a very interesting *localisation transition* at the critical value $n = 1/2$. While the mean squared displacement of the particle increases for large t as $\sim t^{2n-1}$ for $n > 1/2$, it approaches a constant as $t \rightarrow \infty$ for $n < 1/2$. In the marginal case $n = 1/2$, the mean squared displacement grows logarithmically as $\sim \ln t$ at late times. This result is proved analytically by computing the mean squared displacement exactly for all t . This localisation transition also shows up in the full distribution $p_n(x, t)$. We show that for $n < 1/2$, the distribution $p_n(x, t)$ at late times approaches a time-independent form for $|x| \ll t^n$. Moreover, this stationary distribution for $n < 1/2$ has a *double-humped* structure (see Fig. 1). In contrast, for $n \geq 1/2$, the distribution at late times remains time-dependent even for $|x| \ll t^n$ and near its peak at $x = 0$ it approaches a Gaussian form (see Fig. 1), as in (5) for the white noise driven process. The case $n = 1/2$ is a marginal one, where the typical fluctuations grow as $\ln t$ at late times and the distribution remains time-dependent even at late times.

In this paper, we also demonstrate analytically that the distribution $p_n(x, t)$, supported inside the light cone $x \in [-x^*(t), x^*(t)]$ with $x^*(t) = v_0 t^n / \Gamma(n + 1)$, exhibits a large deviation behaviour

$$p_n(x, t) \sim \exp \left[-\gamma t \Phi_n \left(\frac{x}{x^*(t)} \right) \right]. \quad (13)$$

We compute the large deviation rate function $\Phi_n(z)$ analytically for all $n > 0$ which recovers (10) for $n = 1$. The large deviation form in (13) holds when $x \sim x^*(t) \sim t^n$. For $n \geq 1/2$, (13) turns out to hold for much smaller $|x|$, i.e., even when $|x| \sim t^{n-1/2}$ and indeed matches smoothly with the central Gaussian peak describing typical fluctuations. In contrast, for $n < 1/2$, Eq. (13) only describes the behaviour of the distribution near the two light cones $x \sim \pm x^*(t)$, but does not describe the stationary double-humped structure near the centre. It does predict however that for $0 < n < 1/2$, the stationary distribution at late times has super-exponential tails, $-\ln p_n(x, t \rightarrow \infty) \sim |x|^{1/n}$ as $|x| \rightarrow \infty$. For convenience, we provide a summary of our main results and formulae in Section II.

Thus one of our main findings for the process (12) is the emergence of a localised phase for $0 < n < 1/2$ due to the finite memory of the driving noise. This localised phase induced by the active telegraphic noise has no analogue in the passive white noise driven process in (3). One may wonder if there is a physical system that corresponds to this new localised phase for $0 < n < 1/2$. Indeed there is an interesting physical system that corresponds precisely to this $0 < n < 1/2$ case, as we briefly discuss now.

We consider an elastic interface of height $h(\mathbf{x}, t)$ on a d -dimensional substrate. An external time-dependent force $f(t)$ is applied locally, say at the origin. The energy of a height configuration is then given by

$$E[\{h(\mathbf{x}, t)\}] = \int d\mathbf{x} \left[\frac{\kappa}{2} (\nabla h)^2 - f(t) h(\mathbf{x}) \delta(\mathbf{x}) \right]. \quad (14)$$

The first term represents the surface energy with stiffness $\kappa > 0$ and the second term is due to the applied force at the origin. Consider the generic zero temperature (noiseless) dynamics of the interface [2, 6]

$$\frac{\partial h(\mathbf{x}, t)}{\partial t} = -[-\nabla^2]^{z_D} \frac{\delta E[h]}{\delta h} = [-\nabla^2]^{z_D} [\kappa \nabla^2 h(\mathbf{x}, t) + f(t) \delta(\mathbf{x})], \quad (15)$$

where $z_D \geq 0$ is an exponent that parametrizes the dynamics. For example, $z_D = 0$ for the standard model A type dynamics [41], while $z_D = 2$ for the model B dynamics [41] where the total height is conserved. At finite temperature, one may add a thermal additive noise on the right hand side of (15), but we restrict here to zero temperature for simplicity. Since (15) is linear in h , it can be solved using the spatial Fourier transform of the height: $\tilde{h}(\mathbf{k}, t) = \int_{-\infty}^{\infty} d\mathbf{x} \exp(-i\mathbf{k} \cdot \mathbf{x}) h(\mathbf{x}, t)$. Taking the Fourier transform of (15) gives

$$\frac{\partial \tilde{h}(\mathbf{k}, t)}{\partial t} = -\kappa |k|^{2+z_D} \tilde{h}(\mathbf{k}, t) + f(t) |k|^{z_D}. \quad (16)$$

Assuming we start from a flat initial condition $h(\mathbf{x}, 0) = 0$, one finds the explicit solution for general force $f(t)$ as

$$\tilde{h}(\mathbf{k}, t) = \int_0^t ds \exp(-\kappa(t-s)|k|^{2+z_D}) |k|^{z_D} f(s). \quad (17)$$

The position $h(0, t)$ of the point where the force is applied is then given by

$$\begin{aligned} h(0, t) &= \frac{1}{(2\pi)^d} \int d\mathbf{k} \int_0^t ds \exp(-\kappa(t-s)|k|^{z_D+2}) |k|^{z_D} f(s) \\ &= \frac{d \Gamma(\frac{d+z_D}{2+z_D})}{(2+z_D) \Gamma(\frac{d}{2}+1) 2^d \pi^{\frac{d}{2}} \kappa^{\frac{d+z_D}{2+z_D}}} \int_0^t ds (t-s)^{-\frac{d+z_D}{2+z_D}} f(s). \end{aligned} \quad (18)$$

Consider now the external force to be noisy telegraphic, i.e., $f(t) = v_0 \sigma(t)$. Comparing with (12), we see the correspondence

$$n = \frac{2-d}{2+z_D}. \quad (19)$$

For any $z_D \geq 0$, clearly $n < 1$ in (19) and we thus have a physical realization of the process (12) with $n < 1$. By tuning the exponent z_D (which corresponds to choosing different dynamics of the interface), one can physically realize various values of $n < 1$ of our process in (12).

We also note from (19) that since the process (12) is well defined only for $n > 0$, we must have $d < 2$. Thus the most relevant ‘physical’ dimension is $d = 1$, where $n = 1/(2+z_D)$. Indeed, in $d = 1$, similar activity driven interface models have been studied recently, in the context of a Rouse polymer chain in the presence of both the Gaussian white noise and the telegraphic noise [42, 43]. These models, in the continuum limit of long chains, correspond precisely to our model with $z_D = 0$ (model-A dynamics), and hence $n = 1/2$. Similarly, by choosing $z_D = 2$ in the interface model (model-B dynamics), we can realize $n = 1/4$. The choice $z_D = 1$, which applies to the effective dynamics of an interface separating two phases each of which is undergoing model-B dynamics, would correspond to $n = 1/3$ in our process.

The rest of our paper is organised as follows. In Section II we provide a quick summary of our main results with the relevant formulae. In Section III, using a simple trick we provide a different representation of the process (12) that allows us to compute the mean squared displacement as well as the one point position distribution $p_n(x, t)$ in a relatively easier fashion. In Section IV, we compute the mean squared displacement explicitly for all $n > 0$ that

already indicates the existence of the localisation transition at $n = 1/2$. In Section V, we derive an exact Feynman-Kac evolution equation for the cumulant generating function of the position distribution. In Section VI, we show how to compute the large deviation behaviour of the cumulant generating function at late times. In Section VII, we extract the large deviation behaviour of $p_n(x, t)$ from that of the cumulant generating function. In Section VIII we confirm our analytical results via numerical simulations, and in particular we discuss the importance sampling method that we use to compute the rate functions characterising the large deviations. Finally we provide some concluding remarks in Section IX. Details of the exact solution of the cumulant generating function for the three special cases $n = 1$, $n = 2$ and $n = 1/2$ are provided in the Appendix.

II. SUMMARY OF MAIN RESULTS

Since the paper is a bit long, it is perhaps useful, for the convenience of the readers, to provide a brief summary of our main results along with the relevant formulae so that they are easily retrievable if needed. This section does precisely that and the actual derivations are provided in later sections and in the Appendix.

Mean squared displacement: For the process (12) with arbitrary $n > 0$, while the mean position vanishes identically, $\langle x(t) \rangle = 0$ (given $x(0) = 0$), the variance or the mean squared displacement is a nontrivial function of t that we have computed exactly. We find that for all $n > 0$

$$V_n(t) = \langle x^2(t) \rangle = \frac{v_0^2}{\Gamma^2(n+1)} t^{2n} {}_2F_2(1, 2n; n+1, 2n+1; -2\gamma t), \quad (20)$$

where ${}_2F_2(a_1, a_2; b_1, b_2; z)$ is the hypergeometric function [44, 45]. At early times $t \ll \gamma^{-1}$, the variance grows as a power law for any $n > 0$

$$V_n(t) = \frac{v_0^2}{\Gamma^2(n+1)} t^{2n} \left[1 - \frac{4n\gamma}{(n+1)(2n+1)} t + O(t^2) \right]. \quad (21)$$

In contrast, the leading large t behaviour depends on the value of n

$$V_n(t) \approx \begin{cases} \frac{v_0^2}{\gamma} \frac{1}{(2n-1)\Gamma^2(n)} t^{2n-1}, & \text{for } n > 1/2 \\ \frac{v_0^2}{\pi\gamma} [\ln(2\gamma t) + \psi_0], & \text{for } n = 1/2 \\ \frac{v_0^2}{(2\gamma)^{2n}} \sec(n\pi), & \text{for } 0 < n < 1/2 \end{cases} \quad (22)$$

where the constant $\psi_0 = -\Gamma'(1/2)/\Gamma(1/2) = 1.96351\dots$

For $n > 1/2$, identifying $v_0^2/\gamma = 2D$, the result in the first line coincides with $\sigma_n^2(t)$ in (4), demonstrating that the generalised RTP process (12) does converge to the process (3) at late times. In contrast, for $n < 1/2$, the variance approaches a constant asymptotically for large t , indicating that the fluctuations become time independent at late times. The case $n = 1/2$ is marginal where the variance grows very slowly as a logarithm at late times. Thus the exact result for the variance already hints at a localisation transition at $n = 1/2$ separating a localised phase at late times for $n < 1/2$ and a growing de-localised phase for $n > 1/2$. Extensive numerical simulations are in perfect agreement with our results (see Section (IV)).

The position distribution $p_n(x, t)$: For simplicity, we start from the initial condition where the particle is located at the origin $x = 0$ at $t = 0$, and the initial orientation $\sigma(0) = \pm 1$ with equal probability $1/2$. For any $n > 0$, the position distribution $p_n(x, t)$ at time t is symmetric in x and is supported over the interval $x \in [-x^*(t), x^*(t)]$ where

$$x^*(t) = \frac{v_0}{\Gamma(n+1)} t^n. \quad (23)$$

The light cone position $x^*(t)$ in (23) is easy to understand. It corresponds to the rare event when the noise $\sigma(t)$ does not change sign up to time t . If it starts with $\sigma(0) = 1$ (or -1) and does not flip sign up to t , i.e., $\sigma(s) = 1$ (or -1) for all $0 \leq s \leq t$, it follows from (12) that this maximum displacement of the particle is $x^*(t)$ (or $-x^*(t)$) given in (23). The precise form of $p_n(x, t)$ on this support depends however on the value of n . We consider below the two cases $n > 1/2$ and $0 < n < 1/2$ separately.

- **The case $n > 1/2$.** In this case, the typical fluctuation of the particle at late times is $x_{\text{typ}}(t) \sim \sqrt{V_n(t)} \sim t^{n-1/2}$ from the first line of (22). In contrast, the maximal displacement on either side of the origin (corresponding to the two edges of the support) gives another larger scale $x^*(t) \sim t^n \gg x_{\text{typ}}(t)$. It turns out that the full distribution $p_n(x, t)$ has these two scales associated to it (see Fig. 1). If we look at the distribution on the typical scale $x \sim x_{\text{typ}}(t) \sim \sqrt{V_n(t)}$, then $p_n(x, t)$ converges for large t to the scaling form

$$p_n(x, t) \approx \frac{1}{\sqrt{V_n(t)}} f\left(\frac{x}{\sqrt{V_n(t)}}\right), \quad \text{where} \quad f(z) = \frac{1}{\sqrt{2\pi}} e^{-z^2/2}, \quad (24)$$

and $V_n(t)$ at late times is given in the first line in (22). Thus as expected, the typical fluctuations are Gaussian at late times and the scaling distribution coincides with (5) upon identifying an effective $D = v_0^2/2\gamma$.

In contrast, for $|x| \sim x^*(t) \gg t^{n-1/2}$, the distribution $p_n(x, t)$ no longer satisfies the scaling form in (24). These large values of $|x|$ represent *atypical* rare fluctuations and the probability distribution of these rare fluctuations are described by the following large deviation form

$$p_n(x, t) \sim \exp\left[-\gamma t \Phi_n\left(\frac{x}{x^*(t)}\right)\right], \quad (25)$$

where we compute the rate function $\Phi_n(z)$ analytically. We find

$$\Phi_n(z) = \max_{-\infty < w < \infty} \left[-z w + 1 - {}_2F_1\left(-\frac{1}{2}, \frac{1}{2(n-1)}; 1 + \frac{1}{2(n-1)}; -n^2 w^2\right) \right], \quad \text{for } n > 1, \quad (26)$$

where ${}_2F_1(a, b; c; z)$ is the hypergeometric function. In contrast

$$\Phi_n(z) = \max_{-\infty < w < \infty} \left[-z w + 1 - |w| {}_2F_1\left(-\frac{1}{2}, \frac{n}{2-2n}; \frac{n-2}{2(n-1)}; -\frac{1}{n^2|w|^2}\right) \right] \quad \text{for } \frac{1}{2} < n < 1. \quad (27)$$

The function $\Phi_n(z)$, for all $n > 1/2$, is symmetric with support in $z \in [-1, 1]$ and has the small z behaviour

$$\Phi_n(z) \simeq \frac{2n-1}{2n^2} z^2 \quad \text{as } z \rightarrow 0. \quad (28)$$

In contrast, as $z \rightarrow 1$ (the $z \rightarrow -1$ behaviour can be obtained using the symmetry $\Phi_n(z) = \Phi_n(-z)$), the rate function $\Phi_n(z)$ approaches 1 in a singular fashion

$$\Phi_n(z) \simeq \begin{cases} 1 - \frac{2}{\sqrt{2n(2-n)}} (1-z)^{1/2} & \text{for } \frac{1}{2} \leq n < 2 \\ 1 - \left[\Gamma\left(\frac{2n-1}{2(n-1)}\right) \Gamma\left(\frac{n-2}{2(n-1)}\right) \right]^{(n-1)/n} (1-z)^{1/n} & \text{for } n > 2, \end{cases} \quad (29)$$

with logarithmic corrections in the second term for $n = 2$. For small z , substituting (28) in (25) we find that the distribution in the large deviation regime, when extrapolated to small arguments, matches perfectly with the Gaussian distribution describing the typical fluctuations in (24).

- **The case $0 < n < 1/2$.** In this case, we were not able to compute analytically the distribution $p_n(x, t)$ on the typical scale $|x| \sim t^{n-1/2}$. However, we observed numerically that $p_n(x, t)$ becomes time-independent for all $|x| \ll x^*(t) \sim t^n$ at late times. Moreover, this time dependent part near the origin has a double-humped structure (see Fig. 1). The exact result for the variance (in the third line of (22)) is consistent with this time-independent form of $p_n(x, t)$, far inside the light cones. This is the new *localised* phase for $0 < n < 1/2$, whose origin can be traced back to the telegraphic nature of the noise (and has no analogue in the white noise driven process in (2)). However, for large atypical fluctuations when $|x| \sim x^*(t)$ (near the edges), we show that the large deviation form in (25) continues to hold, with the rate function given by

$$\Phi_n(z) = \max_{-\infty < w < \infty} \left[-z w + 1 - |w| {}_2F_1\left(-\frac{1}{2}, \frac{n}{2-2n}; \frac{n-2}{2(n-1)}; -\frac{1}{n^2|w|^2}\right) \right] \quad \text{for } 0 < n < 1/2. \quad (30)$$

which is same as in (27) for $1/2 < n < 1$. However, for $0 < n < 1/2$, the small z behaviour of $\Phi_n(z)$ in (30) is different from that in (28). For $0 < n < 1/2$, the leading small z behaviour of $\Phi_n(z)$ is singular

$$\Phi_n(z) \simeq n \left(\frac{1-n}{g(n)} \right)^{\frac{1}{n}-1} |z|^{\frac{1}{n}} \quad \text{as } z \rightarrow 0, \quad (31)$$

where $g(n) > 0$ is given by

$$g(n) = -\frac{n^{-\frac{n}{n-1}} \Gamma\left(\frac{1}{2(n-1)}\right) \Gamma\left(\frac{n-2}{2(n-1)}\right)}{2\sqrt{\pi}}. \quad (32)$$

For $|z| \rightarrow 1$, the behaviour of $\Phi_n(z)$ in (30) is as in the first line of (29).

For $|x| \ll x^*(t) \sim t^n$, substituting the small z behaviour (31) in (25), we find that the time t drops out and

$$p_n(x, t \rightarrow \infty) \sim \exp\left[-b_n |x|^{1/n}\right], \quad \text{for } 1 \ll |x| \ll t^n \quad (33)$$

where the constant $b_n = \gamma v_0^{-1/n} n ((1-n)/g(n))^{(1-n)/n} (\Gamma(n+1))^{1/n}$. Thus, we see that at late times $p_n(x, t)$ develops time-independent super-exponential tails (since $1/n > 1$ for $0 < n < 1/2$). Thus the large deviation computation also is consistent with the observation that $p_n(x, t)$ does become time-independent at late times for $0 < n < 1/2$, giving rise to the localised phase.

In fact, this double-humped structure of the stationary distribution for $0 < n < 1/2$ can be understood by studying the limit $n \rightarrow 0$. First, for $t \neq s$ one has

$$\lim_{n \rightarrow 0} \frac{1}{\Gamma(n)} (t-s)^{n-1} = 0, \quad (34)$$

since $\Gamma(n)$ has a pole at $n = 0$. We then note that for $\epsilon > 0$,

$$\lim_{n \rightarrow 0} \int_{t-\epsilon}^t ds \frac{1}{\Gamma(n)} (t-s)^{n-1} = \lim_{n \rightarrow 0} \frac{1}{\Gamma(n+1)} \epsilon^n = 1. \quad (35)$$

This means that we can make the identification $\lim_{n \rightarrow 0} \frac{1}{\Gamma(n)} (t-s)^{n-1} = \delta(t-s)$, where $\delta(z)$ is the Dirac delta function. Thus, taking $n \rightarrow 0$ limit in Eq. (12), we see that $x(t) = v_0 \sigma(t)$, i.e. the process $x(t)$ is itself a telegraphic $\pm v_0$ noise. Consequently the position distribution $p(x, t)$, assuming equal probabilities for $\sigma(t) = \pm 1$ at equilibrium, is then exactly given by the bimodal solution

$$p_0(x, t) = \frac{1}{2} \delta(x - v_0) + \frac{1}{2} \delta(x + v_0), \quad (36)$$

for all t . This gives the variance $V_0(t) = v_0^2$, in agreement with the third line in Eq. (22) in the limit $n \rightarrow 0$. We thus see that the double-humped structure seen in general for $n < 1/2$ is a *smear*ed version of what happens in the limiting case $n \rightarrow 0$.

Exact cumulant generating function for special values of n : We managed to compute explicitly the cumulant generating function $U^{(n)}(t; \mu) = \langle e^{-\mu x(t)} \rangle$ of the process at all times t for three special values of n , namely $n = 1$, $n = 2$ and $n = 1/2$. They are derived in the Appendix: Eq. (A2) for $n = 1$, Eq. (A21) for $n = 2$ and Eq. (A36) for $n = 1/2$. While the result for $n = 1$ was known earlier, the other two are new results.

III. THE TRICK

We consider the process (12), defined for arbitrary $n > 0$, and we are interested in the one point marginal distribution of this process at fixed t , i.e. the position distribution $p_n(x, t)$. In general, the computation of this distribution is not easy for general $n > 0$. In this section, we show how it can be made easier using a simple trick. Let us first re-write (12) following the change of variable $s \rightarrow t - s$, as

$$x(t) = \frac{v_0}{\Gamma(n)} \int_0^t ds s^{n-1} \sigma(t-s). \quad (37)$$

Let us now define another auxiliary process $\tilde{x}(t)$ as

$$\tilde{x}(t) = \frac{v_0}{\Gamma(n)} \int_0^t ds s^{n-1} \sigma(s). \quad (38)$$

The process $\tilde{x}(t)$ satisfies the stochastic equation

$$\frac{d\tilde{x}}{dt} = \frac{v_0}{\Gamma(n)} t^{n-1} \sigma(t), \quad (39)$$

which is clearly different from (11) satisfied by the original process $x(t)$. However, as we argue now, the *one point marginal* distribution at fixed t for the two processes $x(t)$ and $\tilde{x}(t)$ are identical

$$\text{Prob.}[x(t) = x, t] = \text{Prob.}[\tilde{x}(t) = x, t]. \quad (40)$$

This equivalence holds as long as the noise process $\sigma(t)$ is in equilibrium.

The equivalence (40) can be proved very simply as follows. Consider the cumulant generating function of the process $x(t)$ in (37)

$$\langle e^{-\mu x(t)} \rangle = \int_{-\infty}^{\infty} e^{-\mu x} p_n(x, t) dx = \langle e^{-\mu \frac{v_0}{\Gamma(n)} \int_0^t ds s^{n-1} \sigma(t-s)} \rangle. \quad (41)$$

Expanding the exponential in a Taylor series we get

$$\langle e^{-\mu x(t)} \rangle = \sum_{k=0}^{\infty} \frac{1}{k!} \left(-\frac{\mu v_0}{\Gamma(n)} \right)^k \int_0^t \cdots \int_0^t ds_1 \dots ds_k s_1^{n-1} \dots s_k^{n-1} \langle \sigma(t-s_1) \sigma(t-s_2) \dots \sigma(t-s_k) \rangle. \quad (42)$$

If the noise $\sigma(t)$ is in equilibrium (which we will assume henceforth), by definition

$$\langle \sigma(t-s_1) \sigma(t-s_2) \dots \sigma(t-s_k) \rangle = \langle \sigma(s_1) \sigma(s_2) \dots \sigma(s_k) \rangle, \quad (43)$$

which follows from the time-reversal symmetry and the stationarity property of the noise process $\sigma(t)$ when it is in equilibrium. Substituting it back into (42) and reconstituting the exponential we arrive at the identity

$$\langle e^{-\mu x(t)} \rangle = \langle e^{-\mu \frac{v_0}{\Gamma(n)} \int_0^t ds s^{n-1} \sigma(s)} \rangle = \langle e^{-\mu \tilde{x}(t)} \rangle \quad (44)$$

where we used the definition of $\tilde{x}(t)$ in (38). Since this equality holds for arbitrary μ , it follows immediately that for all t

$$p_n(x(t) = x, t) = p_n(\tilde{x}(t) = x, t). \quad (45)$$

Let us remark that this equivalence between $x(t)$ and $\tilde{x}(t)$ holds even when the driving noise is white and not necessarily telegraphic. The equivalence (45) requires that the driving noise is in equilibrium, but otherwise holds quite generically. Note however that this equivalence holds only for the one point marginal distribution. The two or higher order marginals of the two processes are evidently different. For example, even the two-time correlation function of the two processes are not identical: $\langle x(t_1)x(t_2) \rangle \neq \langle \tilde{x}(t_1)\tilde{x}(t_2) \rangle$.

Since in this paper we are only interested in the one point distribution $p_n(x, t)$, we can work with the auxiliary process $\tilde{x}(t)$ defined in (38) or equivalently in (39) instead of the original process $x(t)$ in (37). We will see later that the process $\tilde{x}(t)$ is much simpler to study than $x(t)$. For convenience of notation, henceforth we will refer to the process $\tilde{x}(t)$ in (38) by $x(t)$.

IV. EXACT RESULT FOR THE MEAN SQUARED DISPLACEMENT

As a prior to computing the full distribution $p_n(x, t)$ of the process in (38), let us first calculate its second moment (the first moment is trivially zero since $\langle \sigma(t) \rangle = 0$). Squaring (38) and taking average we get

$$V_n(t) = \langle x^2(t) \rangle = \langle \tilde{x}^2(t) \rangle = \frac{v_0^2}{\Gamma^2(n)} \int_0^t \int_0^t ds_1 ds_2 s_1^{n-1} s_2^{n-1} \langle \sigma(s_1) \sigma(s_2) \rangle. \quad (46)$$

Hence we need to compute the two-time correlation function of the telegraphic noise $C(s_1, s_2) = \langle \sigma(s_1) \sigma(s_2) \rangle$. Since we assume that the noise is in equilibrium, $C(s_1, s_2) = C(|s_1 - s_2|)$. The correlation function $C(s)$ can be trivially computed as follows. Consider the product $\sigma(s_1) \sigma(s_1 + s)$. This product is 1 if the noise has the same value at the

two times s_1 and $s_1 + s$, otherwise it is -1 . As we change the time from s to $s + ds$, the change in this product is either 0 (if the noise does not flip in ds) or -2 if the noise flips sign in the interval ds . Thus

$$\sigma(s_1)\sigma(s_1 + s + ds) - \sigma(s_1)\sigma(s_1 + s) = \begin{cases} -2 & \text{with prob. } \gamma ds \\ 0 & \text{with prob. } 1 - \gamma ds. \end{cases} \quad (47)$$

Taking average, dividing by ds , followed by taking the limit $ds \rightarrow 0$ gives $dC(s)/ds = -2\gamma$. Solving, using $C(0) = 1$, we get for all s

$$C(s) = \langle \sigma(s_1)\sigma(s_1 + s) \rangle = e^{-2\gamma|s|}. \quad (48)$$

Substituting (48) in (46) gives

$$V_n(t) = \frac{v_0^2}{\Gamma^2(n)} \int_0^t \int_0^t ds_1 ds_2 s_1^{n-1} s_2^{n-1} e^{-2\gamma|s_1 - s_2|}. \quad (49)$$

Unfortunately, Mathematica was not able to perform this double integral in (49) as it stands. So, we needed to simplify a bit further. Using the symmetry of the integrand under the exchange of s_1 and s_2 , we can re-write it as

$$V_n(t) = \frac{2v_0^2}{\Gamma^2(n)} \int_0^t ds_1 s_1^{n-1} e^{-2\gamma s_1} \int_0^{s_1} ds_2 s_2^{n-1} e^{2\gamma s_2}. \quad (50)$$

Next, in the integral over s_2 , we make the rescaling $s_2 = s_1 u$ to get

$$\begin{aligned} V_n(t) &= \frac{2v_0^2}{\Gamma^2(n)} \int_0^t ds_1 s_1^{2n-1} e^{-2\gamma s_1} \int_0^1 du u^{n-1} e^{2\gamma s_1 u} \\ &= \frac{2v_0^2}{\Gamma^2(n)} \int_0^1 dv (1-v)^{n-1} \int_0^t ds_1 s_1^{2n-1} e^{-2\gamma s_1 v}, \end{aligned} \quad (51)$$

where in going from the first to the second line we made a change of variable $u = 1 - v$. Performing the integral over s_1 explicitly, we arrive at a single integral

$$V_n(t) = \frac{2v_0^2}{(2\gamma)^{2n} \Gamma^2(n)} \int_0^1 dv (1-v)^{n-1} v^{-2n} \gamma(2n, 2\gamma v t), \quad (52)$$

where $\gamma(a, z) = \int_0^z dy y^{a-1} e^{-y}$ is the incomplete gamma function. This single integral in (52) can now be done by Mathematica, leading to our explicit exact result for the variance in (20) in terms of the hypergeometric function. The asymptotic behaviour of $V_n(t)$ for small and large t are already given respectively in (21) and (22). In Fig. 2, we compare our exact result (20) with numerical simulations for $n = 2$, $n = 1/2$ and $n = 1/4$, finding perfect agreement at all times t .

The main consequence of our exact result for the variance is the somewhat surprising fact that for $n < 1/2$, the variance $V_n(t)$ approaches a constant as $t \rightarrow \infty$, leading to the emergence of a localised phase. This is a pure consequence of the finite memory of the telegraphic noise, and does not have any analogue when the driving noise is white, i.e., memoryless.

V. CUMULANT GENERATING FUNCTION VIA FEYNMAN-KAC FORMALISM

Having obtained the second moment exactly, we now turn to the full position distribution $p_n(x, t)$. It is convenient to consider its cumulant generating function. Noting that the noise $\sigma(t)$ at time t can be either $+1$ or -1 , we define the following pair of cumulant generating functions

$$U_{\pm}^{(n)}(t; \mu) = \left\langle \exp \left(-\frac{\mu v_0}{\Gamma(n)} \int_0^t ds s^{n-1} \sigma(s) \right) \delta_{\sigma(t), \pm 1} \right\rangle. \quad (53)$$

which correspond to fixing $\sigma(t) = 1$ and $\sigma(t) = -1$ respectively. The total generating function is given by the sum

$$U^{(n)}(t; \mu) = U_{+}^{(n)}(t; \mu) + U_{-}^{(n)}(t; \mu). \quad (54)$$

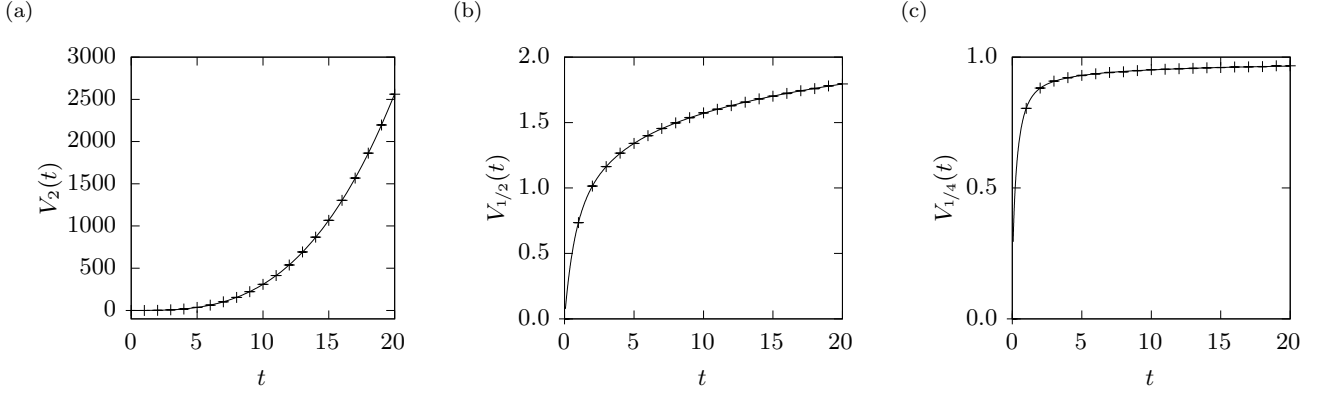


FIG. 2. The numerically obtained variance $V_n(t)$ vs. t (symbols) compared with the theoretical prediction (20) (solid curves) for (a) $n = 2$ (b) $n = 1/2$ and (c) $n = 1/4$. The agreement between theory and simulation is perfect at all times t (the numerical estimate is calculated over 10^7 samples and their error bars are not visible on the scale of the symbols).

Note that we can also write $U^{(n)}(t; \mu)$ as

$$U^{(n)}(t; \mu) = \left\langle e^{-\mu x(t)} \right\rangle = \int_{-\infty}^{\infty} e^{-\mu x} p_n(x, t) dx. \quad (55)$$

In fact, if we set $\mu = ik$, then $U^{(n)}(t; ik)$ is just the Fourier transform of the position distribution at time t .

One can then derive the evolution equations for $U_{\pm}^{(n)}(t; \mu)$ via the Feynman-Kac formalism. Following the same route as in the case of diffusive noise (see e.g. [46]), we advance the time from t and $t + dt$ and keep in mind that in time dt the noise $\sigma(t)$ flips sign with probability γdt and stays in the same state with probability $(1 - \gamma dt)$. We now split the integral inside the exponential in (53) into two parts, one over $[0, t]$ and the other over $[t, t + dt]$. This second part is small and we expand it up to order dt . Finally taking the $dt \rightarrow 0$ limit, we get

$$\frac{dU_{+}^{(n)}}{dt} = - \left(\gamma + \frac{\mu v_0}{\Gamma(n)} t^{n-1} \right) U_{+}^{(n)} + \gamma U_{-}^{(n)} \quad (56)$$

$$\frac{dU_{-}^{(n)}}{dt} = - \left(\gamma - \frac{\mu v_0}{\Gamma(n)} t^{n-1} \right) U_{-}^{(n)} + \gamma U_{+}^{(n)}. \quad (57)$$

They start from the initial conditions,

$$U_{\pm}^{(n)}(t = 0; \mu) = \frac{1}{2}. \quad (58)$$

These initial conditions follow from putting $t = 0$ in the definition (53) and assuming that at $t = 0$, $\sigma(0)$ takes values $+1$ and -1 with equal probability $1/2$. Furthermore we see from the above equations that

$$\left. \frac{dU_{\pm}^{(n)}}{dt} \right|_{t=0} = \mp \frac{1}{2} \frac{\mu v_0}{\Gamma(n)} t^{n-1} \Big|_{t=0}. \quad (59)$$

Thus at $t = 0$, while the derivatives vanish for $n > 1$, they diverge for $n < 1$.

We now rewrite the pair of equations (56) and (57) in terms of $U^{(n)}(t; \mu) = U_{+}^{(n)}(t; \mu) + U_{-}^{(n)}(t; \mu)$ and $W^{(n)}(t; \mu) = U_{+}^{(n)}(t; \mu) - U_{-}^{(n)}(t; \mu)$ which yields

$$\frac{dU^{(n)}}{dt} = - \frac{\mu v_0 t^{n-1}}{\Gamma(n)} W^{(n)} \quad (60)$$

$$\frac{dW^{(n)}}{dt} = -2\gamma W^{(n)} - \frac{\mu v_0 t^{n-1}}{\Gamma(n)} U^{(n)}. \quad (61)$$

They satisfy the initial conditions

$$U^{(n)}(t = 0; \mu) = 1, \quad \text{and} \quad W^{(n)}(t = 0; \mu) = 0. \quad (62)$$

Eliminating $W^{(n)}$ by using Eq. (60) in Eq. (61), yields a closed second order differential equation for $U^{(n)}$

$$\frac{d^2 U^{(n)}}{dt^2} + \left(2\gamma - \frac{(n-1)}{t}\right) \frac{dU^{(n)}}{dt} - \frac{\mu^2 v_0^2 t^{2n-2}}{\Gamma^2(n)} U^{(n)} = 0, \quad (63)$$

valid for all $t \geq 0$ and all $n > 0$. To solve this second order equation, we need two boundary conditions that read

$$U^{(n)}(t=0; \mu) = 1 \quad \text{and} \quad \left. \frac{dU^{(n)}}{dt} \right|_{t=0} = \frac{\mu^2 v_0^2}{n \Gamma^2(n)} t^{2n-1} \Big|_{t=0}. \quad (64)$$

The second condition can be derived by using (62) in (60) and (61) as follows. Substituting $U^{(n)}(t=0; \mu) = 1$ on the right hand side of (61), and solving for $W^{(n)}$ at short times gives to leading order, $W^{(n)}(t; \mu) \approx -(\mu v_0 / \Gamma(n+1)) t^n$. Substituting this in (60) yields the second condition in (64). Thus, for $n > 1/2$, the derivative of $U^{(n)}$ vanish at $t = 0$, while for $n < 1/2$ it diverges. Exactly at $n = 1/2$, the derivative at $t = 0$ is a constant and the initial conditions read

$$U^{(1/2)}(t=0; \mu) = 1 \quad \text{and} \quad \left. \frac{dU^{(1/2)}}{dt} \right|_{t=0} = \frac{2\mu^2 v_0^2}{\pi}. \quad (65)$$

There is an alternative way to arrive at a closed second order differential equation for $U_+^{(n)}(t; \mu)$ and $U_-^{(n)}(t; \mu)$ separately. This second representation turns out to be useful also for deriving the exact result for some values of n , such as $n = 2$ (as shown in the Appendix). To proceed further, it is useful first to write down the pair of equations (56) and (57) in an operator form as follows

$$\hat{L}_+ U_+^{(n)} = \gamma U_-^{(n)}; \quad \text{with} \quad \hat{L}_+ = \frac{d}{dt} + \gamma + \frac{\mu v_0}{\Gamma(n)} t^{n-1} \quad (66)$$

$$\hat{L}_- U_-^{(n)} = \gamma U_+^{(n)}; \quad \text{with} \quad \hat{L}_- = \frac{d}{dt} + \gamma - \frac{\mu v_0}{\Gamma(n)} t^{n-1}. \quad (67)$$

We then operate the first equation from the left by \hat{L}_- and use the second equation to write a closed equation for $U_+^{(n)}(t; \mu)$ only. Similarly, one can obtain a closed equation for $U_-^{(n)}(t; \mu)$ also. We get

$$\hat{L}_- \hat{L}_+ U_+^{(n)} = \gamma^2 U_+^{(n)} \quad (68)$$

$$\hat{L}_+ \hat{L}_- U_-^{(n)} = \gamma^2 U_-^{(n)}. \quad (69)$$

Expanding the operators, we get a pair of ordinary differential equations for $U_{\pm}^{(n)}(t; \mu)$

$$\frac{d^2 U_+^{(n)}}{dt^2} + 2\gamma \frac{dU_+^{(n)}}{dt} + \left(\frac{\mu v_0}{\Gamma(n-1)} t^{n-2} - \frac{\mu^2 v_0^2}{\Gamma^2(n)} t^{2n-2} \right) U_+^{(n)} = 0 \quad (70)$$

$$\frac{d^2 U_-^{(n)}}{dt^2} + 2\gamma \frac{dU_-^{(n)}}{dt} + \left(-\frac{\mu v_0}{\Gamma(n-1)} t^{n-2} - \frac{\mu^2 v_0^2}{\Gamma^2(n)} t^{2n-2} \right) U_-^{(n)} = 0, \quad (71)$$

These equations have to be solved with the initial conditions (58) and (59). It is also clear that the solutions satisfy the following symmetry

$$U_+^{(n)}(t; \mu) = U_-^{(n)}(t; -\mu). \quad (72)$$

Note that in this representation one first solves for $U_+^{(n)}(t; \mu)$ and $U_-^{(n)}(t; \mu)$ separately from Eqs. (70) and (71) and then adds up these solutions to compute $U^{(n)}(t; \mu)$.

For certain specific values of n such as $n = 1$, $n = 2$ and $n = 1/2$, we can solve these differential equations explicitly, as shown in the Appendix. For example, it turns out that for $n = 1$ and $n = 1/2$ one can solve directly the differential equation (63) for $U^{(n)}(t; \mu)$. In contrast, for $n = 2$, it turns out to be more convenient to use the second path, i.e, first solve Eqs. (70) and (71) separately and then add them up. These exact results are presented in the Appendix. For generic n , finding an explicit solution valid at all t seems difficult. However, for large t , one can make progress as we demonstrate in the next section. In particular, for large t and large x , keeping $x/x^*(t)$ fixed (where we recall $x^*(t) = v_0 t^n / \Gamma(n+1)$), we show below how the large deviation properties of $p_n(x, t)$ can be extracted from Eq. (63).

VI. LARGE DEVIATION ANALYSIS OF THE CUMULANT GENERATING FUNCTION

It is easier and perhaps more physical to guess the possible large deviation behaviour of $p_n(x, t)$ in real space x , rather than for its cumulant generating function $U^{(n)}(t; \mu)$. So, our strategy would be to (i) first guess the large deviation form of $p_n(x, t)$ and then use it to anticipate the large deviation form of $U^{(n)}(t; \mu)$ and then (ii) substitute this anticipated form in the differential equation (63) to explicitly derive the large deviation function.

Anticipated large deviation form for $p_n(x, t)$. Let us then first see what we may expect for the large deviation behaviour of $p_n(x, t)$. It is clear that if the noise $v_0 \sigma(t)$ does not flip sign at all in time t , then the maximum distance travelled by the particle is $\pm v_0 t^n / \Gamma(n+1)$ from (38). This is the largest possible deviation in the x direction, and the probability for this event (of no flipping) is clearly $e^{-\gamma t}$. Hence, it is natural to anticipate that in the limit $t \rightarrow \infty$, $x \rightarrow \infty$ but with the ratio $z = \Gamma(n+1)x / (v_0 t^n)$ fixed, the distribution $p_n(x, t)$ exhibits the following large deviation behaviour

$$p_n(x, t) \sim \exp \left[-\gamma t \Phi_n \left(\frac{\Gamma(n+1)x}{v_0 t^n} \right) \right], \quad (73)$$

where $\Phi_n(z)$ is the rate function, which is symmetric in z and is supported over the interval $z \in [-1, 1]$ since $|z|$ can not exceed 1. The probability of the rarest event that $|z| = 1$ is $e^{-\gamma t}$, i.e., the probability that $\sigma(t)$ does not change sign up to time t . Hence, putting $z = 1$ in (73), we also infer that

$$\Phi_n(\pm 1) = 1. \quad (74)$$

Anticipated large deviation form for $U^{(n)}(t; \mu)$. Let us now see what Eq. (73) would imply for the cumulant generating function $U^{(n)}(t; \mu)$ in (55). Substituting the anticipated large deviation behaviour (73) in (55) we get

$$\begin{aligned} U^{(n)}(t; \mu) &= \int_{-\infty}^{\infty} dx p_n(x, t) e^{-\mu x} \\ &\sim \int_{-1}^1 dz e^{-\gamma t \Phi_n(z) - \frac{\mu v_0 t^n}{\Gamma(n+1)} z} \\ &\sim \int_{-1}^1 dz e^{-\gamma t [w z + \Phi_n(z)]}; \quad \text{with } w = \frac{\mu v_0 t^{n-1}}{\Gamma(n+1)\gamma} \end{aligned} \quad (75)$$

where, in going from the first to the second line, we made the change of variable $x = (v_0 t^n / \Gamma(n+1)) z$, and we did not keep track of pre-exponential factors.

We now take the limit $t \rightarrow \infty$ and $\mu \rightarrow 0$ for $n > 1$ (or $\mu \rightarrow \infty$ for $n < 1$), such that $w = \mu v_0 t^{n-1} / (\Gamma(n+1)\gamma)$ remains fixed. Then, for large t , we can estimate the integral in (75) by the saddle point method. This gives

$$U^{(n)}(t; \mu) \sim e^{-\gamma t H_n(w)}; \quad \text{where } H_n(w) = \min_{-1 \leq z \leq 1} [w z + \Phi_n(z)]. \quad (76)$$

Hence, we have our desired large deviation ansatz for $U^{(n)}(t; \mu)$

$$U^{(n)}(t; \mu) \sim \exp \left[-\gamma t H_n \left(\frac{\mu v_0 t^{n-1}}{\Gamma(n+1)\gamma} \right) \right]. \quad (77)$$

Let us now check that this large deviation ansatz (77) is consistent with the extreme trajectories. Consider the limit $\mu \rightarrow \infty$ first. In this limit, from (53), it follows that the extreme paths starting with $\sigma = -1$ that never flip will dominate and contribute

$$U^{(n)}(t; \mu) \sim \exp \left(-\gamma t + \mu \frac{v_0 t^n}{\Gamma(n+1)} \right). \quad (78)$$

Similarly for $\mu \rightarrow -\infty$ we find

$$U^{(n)}(t; \mu) \sim \frac{1}{2} \exp \left(-\gamma t - \mu \frac{v_0 t^n}{\Gamma(n+1)} \right). \quad (79)$$

We note that both (78) and (79) do satisfy the large deviation ansatz in (77) with a predicted asymptotic behaviour of $H_n(w)$ for large $|w|$

$$H_n(w) \approx 1 - |w| \quad (80)$$

Explicit solution for $H_n(w)$. Thus our main conclusion from the above exercise is that the cumulant generating function $U^{(n)}(t; \mu)$ for large t has an anticipated large deviation (77) with $H_n(w)$ denoting the rate function in the w space. To derive $H_n(w)$ explicitly, we substitute the ansatz (77) in the differential equation (63) and obtain

$$\gamma^2 [G_n^2(w) - 2G_n(w) - n^2 w^2] + \frac{1}{t} \gamma (n-1) [G_n(w) - wG_n'(w)] = 0. \quad (81)$$

where

$$G_n(w) = H_n(w) + (n-1) w H_n'(w). \quad (82)$$

Consequently, the leading order term for large t gives

$$G_n^2(w) - 2G_n(w) - n^2 w^2 = 0. \quad (83)$$

Solving the quadratic equation gives a first order differential equation for $H_n(w)$

$$(n-1) w H_n'(w) + H_n(w) = 1 \pm \sqrt{1 + n^2 w^2} \quad (84)$$

where we have the choice of two roots. We now consider the two cases $n > 1$ and $0 < n < 1$ separately, as it will turn out that the solution $H_n(w)$ has different forms in these two cases.

- **The case $n > 1$.** In this case, as $t \rightarrow \infty$, in order to keep $w = \mu v_0 t^{n-1} / \gamma \Gamma(n+1)$ fixed, we must have $\mu \rightarrow 0$. Solving the first-order equation (84) gives the general solution

$$H_n(w) = \frac{w^{-1/(n-1)}}{n-1} \left[c + \int_0^w \left(1 \pm \sqrt{1 + n^2 x^2} \right) x^{(2-n)/(n-1)} dx \right], \quad (85)$$

where c is an integration constant. To determine c and the sign of the root to be chosen we note that we must have $H_n(w \rightarrow 0) = 0$, which follows from the fact that $U^{(n)}(t; \mu = 0) = 1$ for all t . However by symmetry of the probability distribution we also have $H_n'(0) = 0$. Examining Eq. (84) then shows that we should choose the negative root. We thus find

$$H_n(w) = \frac{w^{-1/(n-1)}}{n-1} \left[c + \int_0^w \left(1 - \sqrt{1 + n^2 x^2} \right) x^{(2-n)/(n-1)} dx \right], \quad (86)$$

and with this choice of sign we see that the integrand in (86) for small x behaves as $x^{\frac{n}{n-1}}$ and the integral is thus convergent around $x = 0$ if $n > 1$. For small w we thus find

$$H_n(w) = c \frac{w^{-1/(n-1)}}{n-1} - \frac{n^2}{2(2n-1)} w^2, \quad (87)$$

and from this we conclude that $c = 0$ since $H_n(w \rightarrow 0) = 0$. Setting $c = 0$ and performing the integral explicitly in (86) we get for $n > 1$

$$H_n(w) = 1 - {}_2F_1 \left(-\frac{1}{2}, \frac{1}{2(n-1)}; 1 + \frac{1}{2(n-1)}; -n^2 w^2 \right), \quad (88)$$

where ${}_2F_1(a, b; c; z)$ is the hypergeometric function [45]. For $n = 1$ and $n = 2$ one obtains rather simple expressions

$$H_1(w) = 1 - \sqrt{1 + w^2} \quad (89)$$

$$H_2(w) = 1 - \frac{1}{2} \sqrt{1 + 4w^2} - \frac{\operatorname{arcsinh}(2w)}{4w}. \quad (90)$$

The function $H_n(w)$ in (88) is clearly symmetric around $w = 0$, i.e., $H_n(w) = H_n(-w)$. The small w asymptotic behaviour of $H_n(w)$ is easy to derive and we get for all $n \geq 1$

$$H_n(w) = -\frac{n^2}{2(2n-1)} w^2 + \frac{n^4}{8(4n-3)} w^4 - \frac{n^6}{16(6n-5)} w^6 + O(w^8) \quad \text{as } w \rightarrow 0. \quad (91)$$

In contrast, the large w asymptotics of $H_n(w)$ depends on whether $n < 2$ or $n > 2$. We get as $w \rightarrow \infty$

$$H_n(w) = \begin{cases} -w + 1 - \frac{1}{2n(2-n)} \frac{1}{w} + \dots & \text{for } 1 \leq n < 2 \\ -w + 1 - (n-1) \Gamma\left(\frac{2n-1}{2(n-1)}\right) \Gamma\left(\frac{n-2}{2(n-1)}\right) n^{-n/(n-1)} w^{-1/(n-1)} + \dots & \text{for } n > 2. \end{cases} \quad (92)$$

- **The case $0 < n < 1$.** In this case if we consider the limit where $t \rightarrow \infty$ while $w = \mu v_0 t^{n-1}/(\Gamma(n+1)\gamma)$ is held fixed, this implies that we are considering the limit where $\mu \rightarrow \infty$. Thus even when w is small one is still in the limit where $\mu \rightarrow \infty$. This means that we can no longer use the boundary condition at $\mu = 0$ or $w = 0$ as in the case $n > 1$. Instead we have to use the asymptotic boundary condition in Eq. (80) as $|w| \rightarrow \infty$ to determine the behaviour of $H_n(w)$ for w finite (precisely the opposite of what we have done for $n > 1$). now, the general solution of the first-order differential equation (84) can also be written as

$$H_n(w) = \frac{-w^{-1/(n-1)}}{n-1} \left[c_1 + \int_w^\infty \left(1 \pm \sqrt{1+n^2 x^2} \right) x^{(2-n)/(n-1)} dx \right], \quad (93)$$

where c_1 is the integration constant. next, we note that for large w the indefinite form of the integral appearing in Eq. (93)

$$I_\pm(w) = \int^w dx \left(1 \pm \sqrt{1+n^2 x^2} \right) x^{(2-n)/(n-1)} \approx (n-1) \left[w^{\frac{1}{(n-1)}} \pm w^{\frac{n}{(n-1)}} \right], \quad (94)$$

is convergent as $w \rightarrow \infty$ for $0 < n < 1$. Now, in order to satisfy the boundary condition in Eq. (80), we see using (94) in (93) that we must choose again the negative root above and set $c_1 = 0$ in Eq. (93). This gives

$$H_n(w) = -\frac{w^{-1/(n-1)}}{n-1} \left[\int_w^\infty \left(1 - \sqrt{1+n^2 x^2} \right) x^{(2-n)/(n-1)} dx \right]. \quad (95)$$

The integral above can be evaluated to yield (for $w > 0$)

$$H_n(w) = 1 - w {}_2F_1 \left(-\frac{1}{2}, \frac{n}{2-2n}; \frac{n-2}{2(n-1)}; -\frac{1}{n^2 w^2} \right). \quad (96)$$

The solution for $w < 0$ can be similarly obtained. In fact, since $H_n(w)$ is symmetric, the solution for all w is given by

$$H_n(w) = 1 - |w| {}_2F_1 \left(-\frac{1}{2}, \frac{n}{2-2n}; \frac{n-2}{2(n-1)}; -\frac{1}{n^2 w^2} \right). \quad (97)$$

This solution has the large w expansion

$$H_n(w) = 1 - |w| - \frac{1}{2n(2-n)|w|} + \dots, \quad (98)$$

that coincides with the large w expansion for the case $1 \leq n < 2$ given in Eq. (92). The small w expansion is given by

$$H_n(w) = \frac{n^{-\frac{n}{n-1}} \Gamma\left(\frac{1}{2(n-1)}\right) \Gamma\left(\frac{n-2}{2(n-1)}\right)}{2\sqrt{\pi}} |w|^{\frac{1}{1-n}} - \frac{n^2}{2(2n-1)} w^2 + \frac{n^4}{8(4n-3)} w^4 - \frac{n^6}{16(6n-5)} w^6 + O(w^8). \quad (99)$$

This has the same analytic terms as the expansion Eq. (91) which is valid for the case $n > 1$ but the first term is non-analytic, proportional to $|w|^{\frac{1}{1-n}}$ which appears only for $0 < n < 1$. In the case $n > 1/2$, the leading correction to $H_n(w)$ at small w is still of order w^2 , however for $n < 1/2$ it is the term proportional to $|w|^{\frac{1}{1-n}}$. Therefore at lowest order for small w we find

$$H_n(w) = \begin{cases} -\frac{n^2}{2(2n-1)} w^2 + \dots & \text{for } \frac{1}{2} < n \leq 1 \\ -g(n)|w|^{\frac{1}{1-n}} + \dots & \text{for } 0 < n < \frac{1}{2}. \end{cases} \quad (100)$$

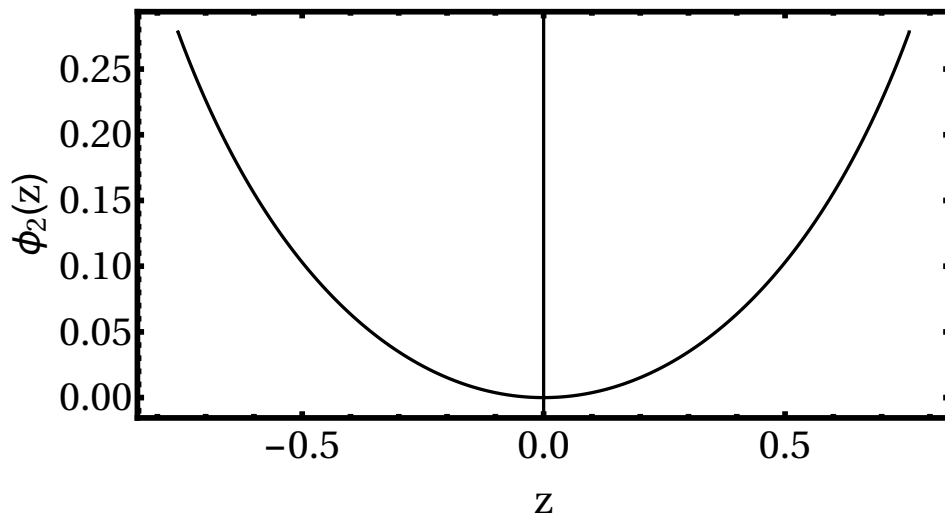


FIG. 3. The rate function $\Phi_2(z)$ vs. z obtained parametrically from Eq. (105) for $n = 2$. The function $\Phi_2(z)$ is symmetric around $z = 0$ and is supported over $z \in [-1, 1]$.

where

$$g(n) = -\frac{n^{-\frac{n}{n-1}} \Gamma\left(\frac{1}{2(n-1)}\right) \Gamma\left(\frac{n-2}{2(n-1)}\right)}{2\sqrt{\pi}}, \quad (101)$$

and one can check that $g(n) > 0$ for $0 < n < \frac{1}{2}$.

Finally, we note that exactly at $n = 1/2$, (97) has a simpler expression

$$H_{1/2}(w) = 1 - \frac{1}{2} \sqrt{w^2 + 4} - \frac{w^2}{4} \operatorname{arcsinh}\left(\frac{2}{|w|}\right). \quad (102)$$

For small w , we get $H_{1/2}(w) \approx -w^2 \ln |w|/4$ to leading order, while for large $|w|$, $H_{1/2}(w) \approx 1 - |w|$.

VII. EXTRACTING THE LARGE DEVIATION BEHAVIOUR OF $p_n(x, t)$

We have already seen that on the scale $x \sim x^*(t) = v_0 t^n / \Gamma(n+1)$, the distribution $p_n(x, t)$ has the large deviation form in (73) where the rate function $\Phi_n(z)$ is related to $H_n(w)$ via the Legendre transform in (76). Formally inverting this Legendre transform we get

$$\Phi_n(z) = \max_{-\infty < w < \infty} [-z w + H_n(w)], \quad (103)$$

where $H_n(w)$ is known explicitly from (88) for $n > 1$ and (97) for $0 < n < 1$. As an example, consider first $n = 1$ for which $H_1(w) = 1 - \sqrt{1 + w^2}$ from (89). Maximizing (103) gives

$$\Phi_1(z) = 1 - \sqrt{1 - z^2} \quad -1 \leq z \leq 1, \quad (104)$$

which thus reproduces the result (10) quoted in the introduction. For generic n , it is difficult to obtain $\Phi_n(z)$ explicitly. However, by maximising the function inside the parenthesis in (103) with respect to w , we can express $\Phi_n(z)$ in the following parametric form that can be easily plotted in Mathematica

$$\begin{aligned} z &= H'_n(w) \\ \Phi_n &= -w H'_n(w) + H_n(w). \end{aligned} \quad (105)$$

As an example, consider $n = 2$ for which $H_2(w)$ is given explicitly in (90). Using this in (105), we plot $\Phi_2(z)$ vs. z in Fig. 3.

The rate function is symmetrically supported over the interval $z \in [-1, 1]$. The asymptotic behaviors of $\Phi_n(z)$ as $z \rightarrow 0$ and $z \rightarrow \pm 1$ can be obtained from (103) by substituting the $w \rightarrow 0$ and $w \rightarrow \mp\infty$ behaviors of $H_n(w)$ detailed in the previous section. This leads to the results quoted in the summary in Section II.

To verify our analytical prediction for $\Phi_n(z)$ in (103) we have done extensive simulations using a nontrivial importance sampling algorithm that is described in detail in the next section. The simulation results are in excellent agreement with our analytical predictions.

VIII. NUMERICAL SIMULATIONS

Here we compare the analytical results of the previous sections with numerical simulations. We first describe the method of simulation and in particular the crucial idea of importance sampling. We then carry out the comparison between numerics and analytics.

A. The Method

Performing computer simulations to study any model, requires a suitable discretisation of the model. Fortunately in this case, an exact discretisation is possible. We use for all values of n the representation (38) which can be exactly discretised by a piecewise solution of the integral

$$x(t) = \frac{v_0}{\Gamma(n+1)} \sum_i \sigma_i (t_{i+1}^n - t_i^n), \quad (106)$$

where the sum goes over all flips, such that the σ_i alternate between $+1$ and -1 .

Now we can generate independent samples of this process for arbitrary t by drawing the times until the next flip τ_i from an exponential distribution $P(\tau) = \gamma \exp(-\gamma \tau)$ until $\sum_i \tau_i \geq t$. The last waiting time is truncated to enforce $\sum_i \tau_i = t$. Note that the number of flips fluctuates.

To obtain numerical estimates for the rate function, it is necessary to calculate the probability density function, especially including the far tails of extremely rare events which occur with probabilities of less than, say, 10^{-100} . It is infeasible with current computers to generate the order of 10^{100} samples, which are necessary to observe such an event once on average—much less to generate enough of those rare events to allow an estimate of their probability with reasonable statistical precision.

Therefore, we need to resort to more sophisticated Markov chain Monte Carlo simulation techniques. The basic idea is to generate samples which are biased in a controlled way to increase the chance to encounter a very rare event, thus allowing to collect robust statistics of this event. Since the bias is well controlled, one can obtain the unbiased probability density from these measurements. This fundamental concept is also known as *importance sampling*.

To generate samples with a well controlled bias, we use the *Metropolis-Hastings* algorithm [47]. Therefore we construct a Markov chain of configurations, in our case the vector of times between flips τ_i . To generate the next link τ_{i+1} in the Markov chain, we propose a configuration τ' generated by applying a small change to the current configuration τ_i and accept it according to an acceptance probability $p_{\text{acc}}(\tau_i \rightarrow \tau')$. If the new configuration is accepted $\tau_{i+1} = \tau'$, otherwise the old configuration is repeated in the chain, i.e. $\tau_{i+1} = \tau_i$. The acceptance probability needs to be chosen such that detailed balance holds. The exact choice then determines according to which distribution the configurations will appear eventually in the Markov chain. The change move in our case is to select a random component τ_i^* and replacing it with a new random time drawn from the same exponential distribution, or flip the initial direction σ_0 . Note that this might change the number of τ_i defining the configuration: if the newly generated τ_i^* is larger, the last few τ_i might need to be removed and if τ_i^* becomes smaller, a few more flips might need to happen before the time t is reached. Also this change move allows to reach every possible configuration after enough changes, which means that ergodicity holds, the second prerequisite necessary for a Markov chain to generate configurations according to the desired distribution.

Here we use for the acceptance probability the original choice generating Boltzmann distributed states $p_{\text{acc}} = \min(1, e^{-\Delta x/T})$ [48], i.e. configurations in the Markov chain will be distributed according to

$$Q_T(\tau) = \frac{1}{Z_T} e^{-x(\tau)/T} Q(\tau), \quad (107)$$

where Q is the natural distribution and Z_T the partition function necessary for normalization. The “temperature” T is in this context just a free parameter, which we can use to bias the resulting samples: small temperatures will lead to small “energies” x , large T lead to typical values of x and small negative T lead to large values of x .

We can estimate the probability density $p_T(x)$ of our artificial temperature ensemble and remove the bias to get the unbiased distribution in a range of very atypical x but with good statistics [49]. Using Eq. (107) we see

$$p_T(x) = \sum_{\{\tau|x(\tau)=x\}} Q_T(\tau) \quad (108)$$

$$= \sum_{\{\tau|x(\tau)=x\}} \frac{1}{Z_T} e^{-x(\tau)/T} Q(\tau) \quad (109)$$

$$= \frac{1}{Z_T} e^{-x/T} p(x), \quad (110)$$

where $p(x)$ is the searched for, unbiased distribution. This means that we need the partition function Z_T to correct the bias. Fortunately, we can use that $p(x)$ needs to be unique if derived for the same x but different T . So we need to simulate and estimate $p_T(x)$ for multiple, carefully chosen values of T , such that the different $p_T(x)$ overlap. Then the ratio of the Z_T of overlapping ranges can be determined using

$$p_{T_j}(x) e^{x/T_j} Z_{T_j} = p_{T_i}(x) e^{x/T_i} Z_{T_i}. \quad (111)$$

The absolute values of the Z_T are then obtained by normalization of the full distribution $p(x)$.

As usual for Markov chain Monte Carlo, care has to be taken that the Markov chain is equilibrated before taking measurements and the correlation between two samples has to be considered to avoid underestimation of the statistical error [50]. Generally, this method works quite well for a wide range of problems [51–54], especially it was already applied in the context of the run-and-tumble particle, the $n = 1$ case of the model at hand [55].

B. Comparison of analytical and numerical results

First, we generated 10^7 independent trajectories and measured their positions at time t to obtain estimates for the variance $V_n(t) = \langle x^2(t) \rangle$ shown in Fig. 2 as well as an estimate for the distribution $p_n(x, t)$ shown in Fig. 1.

Obtaining an estimate for the rate function $\Phi_n(z)$, where $z = x/x^*(t)$ with $x^*(t) = v_0 t^n / \Gamma(n + 1)$, is more complicated, since we need to have high precision data for the tails of $p_n(x, t)$. We obtain those for multiple values of t using the Markov chain Monte Carlo method described above and from this calculate *empirical* rate functions and compare them to the expressions from Eqs. (26) and (27) in Fig. 4. The symbols represent the results of our Monte Carlo simulations and the lines are obtained by numerical maximization of Eqs. (26) and (27). Note that the values of t we simulated are already large enough to coincide with the apparent asymptotic form within statistical precision, since all values collapse onto the asymptotic form.

We see a very good agreement over most of the support of the rate function. The slight deviation from the predicted rate function in the extreme tail is caused by difficulties to reach equilibrium, caused by this extremely steep tail of extremely rare events. In the inset of Fig. 4(a) we show results obtained with different numerical efforts, after different equilibration times t_{eq} of the Markov chain measured in sweeps, i.e. t change attempts. From this we estimate that we can not reach equilibrium for $z > 0.95$, up to where our two largest simulations coincide. However the numerical data for lower values of z should be of good quality. The very good agreement over most of the rate function confirms the predicted analytical form.

In Fig. 4(b) we show the same comparison for the $n = 1/2$ case, which confirms our analytical rate function convincingly. Also here, we observe the very slight deviation at the very end of the tail, which arises in the same way as for the $n = 2$ case.

In a similar fashion, our results for the rate function of $n = 1/4$ are shown in Fig. 4(c). In this case we could thoroughly sample whole support as well. In contrast to $n \geq 1/2$ we see a clear size dependence of our measurements in the inset, where the double humped structure of finite t is visible but approaches the monotonous form of the rate function with increasing t .

IX. CONCLUSION

In this paper we studied a class of stochastic processes, $x(t) = \int_0^t ds (t-s)^{n-1} \xi(s)$ indexed by $n > 0$. When the driving noise $\xi(t)$ is an uncorrelated Gaussian white noise (the so called ‘passive’ process), the position distribution $p_n(x, t)$ of $x(t)$ is trivially Gaussian at all times for all $n > 1/2$. The main purpose of this paper was to consider the case when the driving noise $\xi(t)$ is an ‘active’ noise, i.e., $\xi(t) = (v_0/\Gamma(n)) \sigma(t)$, where $\sigma(t)$ is a telegraphic noise

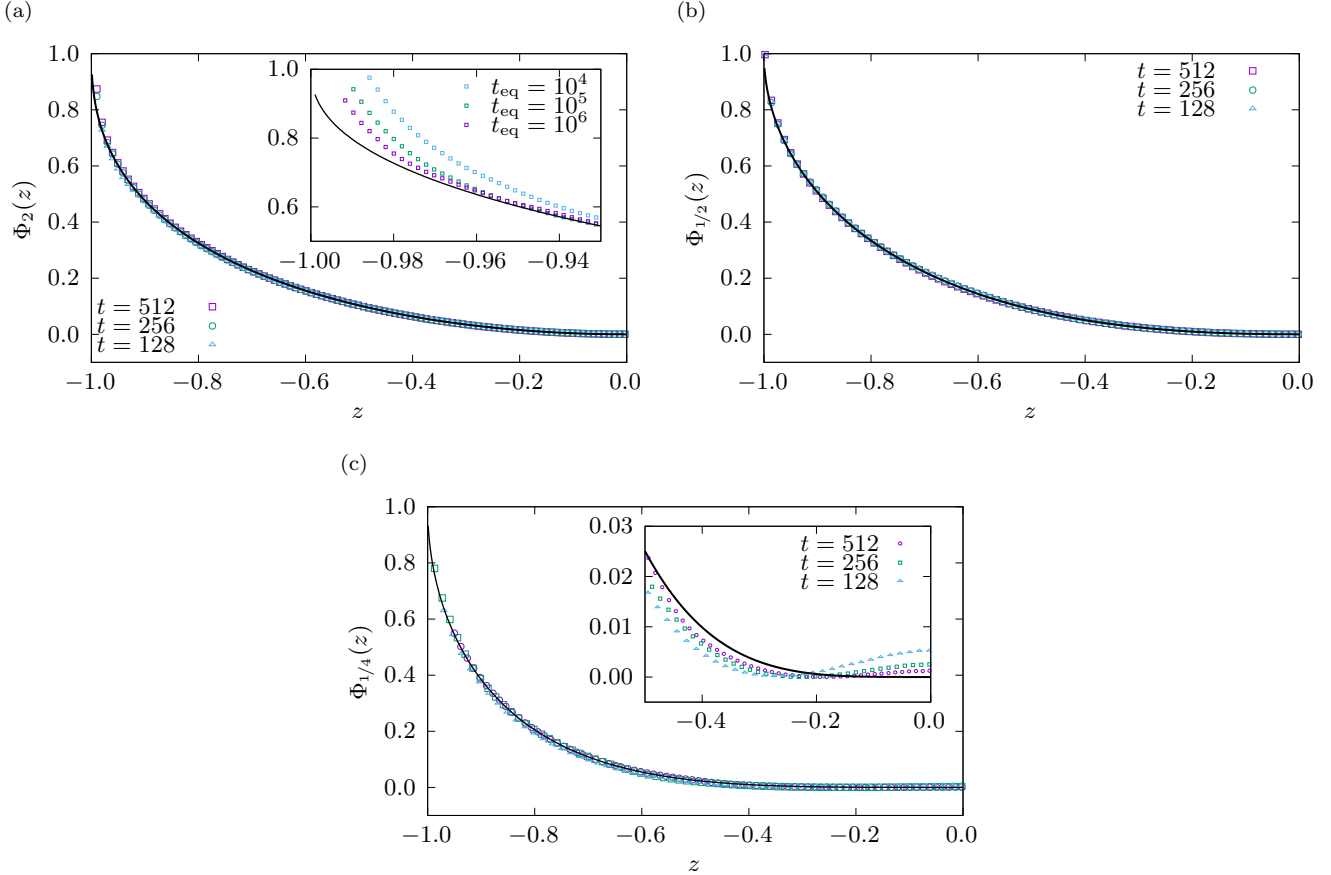


FIG. 4. Estimates for the rate function from simulation at $t \in \{128, 256, 512\}$ estimated from Markov chains of the length of 10^7 sweeps after an equilibration time of 10^6 sweeps at a few dozen different temperatures. At these values of t , there is almost no size dependence anymore such that we assume that the results are already almost converged to the actual rate function, which describes the $t \rightarrow \infty$ limit. The rate function estimates are due to symmetry and to conserve computing power only shown for the left branch. All empirical rate functions are shifted such that their minimum is at zero. (a) The case $n = 2$. The inset shows for $t = 512$ that higher numerical precision leads to results closer to the analytical expectation. (b) The $n = 1/2$ case. The same slight deviation at the very end of the tail occurs as for the $n = 2$ case. (c) The case $n = 1/4$. The inset shows a zoom to illustrate the convergence of the two peak structure of $p_n(x, t)$ towards the flat shape of the rate function $\Phi_n(z)$.

switching between two values ± 1 at a constant rate γ . Unlike in the passive case, the position distribution $p_n(x, t)$ in the active case is well defined for all $n > 0$, is highly non-Gaussian and nontrivial to compute. For $n = 1$, our process reduces to the standard run and tumble process in one dimension. By computing the mean squared displacement exactly, we found that a localised phase emerges for $0 < n < 1/2$ where the variance approaches a constant at late times. This localised phase owes its origin to the finite memory of the active noise, and has no analogue in the corresponding passive white noise driven process. For $n > 1/2$, the variance grows at late times as $\sim t^{n-1/2}$. In the critical case $n = 1/2$, the variance grows slowly as $\ln t$ at late times.

This localisation transition is also confirmed from the study of the position distribution $p_n(x, t)$ at late times. We have shown that for $n < 1/2$, the position distribution approaches a stationary form with a double-humped structure at late times, while for $n \geq 1/2$ the distribution remains time dependent even at late times. Furthermore, we have shown that the tails of the position distribution can be described by the large deviation form: $p_n(x, t) \sim \exp\left[-\gamma t \Phi_n\left(\frac{x}{x^*(t)}\right)\right]$ where $x^*(t) = v_0 t^n / \Gamma(n + 1)$. We computed the large deviation function $\Phi_n(z)$ analytically for all n and verified it numerically using an importance sampling algorithm. One of the predictions of our exact computation is that in the localised phase $n < 1/2$, the stationary distribution has super-exponential tails: $p_n(x, \infty) \sim \exp[-b_n |x|^{1/n}]$ (b_n being a constant) as $|x| \rightarrow \infty$. Computing the full stationary distribution $p_n(x, \infty)$ for all x for $n < 1/2$, in particular an analytical description of the double-humped structure, remains a challenging open problem.

In this paper, we have restricted ourselves only to the one point function $p_n(x, t)$ of the process $x(t)$. It would be interesting to compute the multi-time correlation functions, as well as other observables such as the first-passage

probability for the process $x(t)$ for general $n > 0$.

Appendix A: Exact cumulant generating function for specific values of n

In this Appendix, we show that for certain specific values of n , namely $n = 1$, $n = 2$ and the critical case $n = 1/2$, the cumulant generating function $U^{(n)}(\mu; t)$ of the position distribution $p_n(x, t)$ can be computed exactly.

1. The case $n = 1$

Even though the exact result for $n = 1$ is already known in the literature as mentioned in the introduction, we show here, for the sake of completeness, how the result follows from the formalism presented in the paper. Putting $n = 1$ in Eq. (63) gives

$$\frac{d^2 U^{(1)}}{dt^2} + 2\gamma \frac{dU^{(1)}}{dt} - \mu^2 v_0^2 U^{(1)} = 0, \quad (\text{A1})$$

to be solved with the boundary conditions: (i) $U^{(1)}(t = 0; \mu) = 1$ and (ii) $dU^{(1)}/dt|_{t=0} = 0$. Since this is a second order differential equation with constant coefficients, the solution can be trivially obtained in the form $U^{(1)}(t; \mu) = A_1 e^{\lambda t} + A_2 e^{-\lambda t}$ with $\lambda = -\gamma + \sqrt{\gamma^2 + \mu^2 v_0^2}$. Upon fixing the two unknown constants via the two boundary conditions we get

$$U^{(1)}(t; \mu) = \frac{1}{2} \left[1 + \frac{\gamma}{\sqrt{\gamma^2 + \mu^2 v_0^2}} \right] e^{(\sqrt{\gamma^2 + \mu^2 v_0^2} - \gamma)t} + \frac{1}{2} \left[1 - \frac{\gamma}{\sqrt{\gamma^2 + \mu^2 v_0^2}} \right] e^{-(\sqrt{\gamma^2 + \mu^2 v_0^2} + \gamma)t}. \quad (\text{A2})$$

In the long time limit, the first term dominates over the second term. Ignoring pre-exponential factors, one finds that as $t \rightarrow \infty$

$$U^{(1)}(t; \mu) \sim \exp \left[-\gamma t H_1 \left(w = \frac{\mu v_0}{\gamma} \right) \right]; \quad \text{with} \quad H_1(w) = 1 - \sqrt{1 + w^2}, \quad (\text{A3})$$

in agreement with (89). For finite t , by inverting (A2) with respect to μ , one recovers the known exact distribution $p_1(x, t)$ mentioned in Eq. (9) of the introduction.

2. The case $n = 2$

In this case, setting $n = 2$ in (63) gives the second order differential equation

$$\frac{d^2 U^{(2)}}{dt^2} + \left(2\gamma - \frac{1}{t} \right) \frac{dU^{(2)}}{dt} - \mu^2 v_0^2 t^2 U^{(2)} = 0. \quad (\text{A4})$$

However, we did not succeed in finding the two linearly independent solutions of this equation in terms of standard special functions. Instead, we found that for $n = 2$, we could solve the separate differential equations (70) and (71) for $U_+^{(2)}$ and $U_-^{(2)}$ and then add them up to express the exact solution for $U^{(2)}(t; \mu)$ in terms of standard special functions, in this case the parabolic cylinder functions.

To proceed, Eqs. (70) and (71) for $n = 2$ read

$$\frac{d^2 U_+^{(2)}}{dt^2} + 2\gamma \frac{dU_+^{(2)}}{dt} + (\mu v_0 - \mu^2 v_0^2 t^2) U_+^{(2)} = 0 \quad (\text{A5})$$

$$\frac{d^2 U_-^{(2)}}{dt^2} + 2\gamma \frac{dU_-^{(2)}}{dt} + (-\mu v_0 - \mu^2 v_0^2 t^2) U_-^{(2)} = 0, \quad (\text{A6})$$

to be solved with the boundary conditions

$$U_{\pm}^{(2)}(t = 0; \mu) = \frac{1}{2}; \quad \text{and} \quad \frac{dU_{\pm}^{(2)}}{dt} \Big|_{t=0} = 0. \quad (\text{A7})$$

It is clear that the solutions satisfy the following symmetry

$$U_+^{(2)}(t; \mu) = U_-^{(2)}(t; -\mu). \quad (\text{A8})$$

Below, we will compute $U_\pm(t; \mu)$ explicitly by assuming $\mu \geq 0$. The solution for negative μ can then be obtained from the symmetry relation (A8)

To proceed further, we make the following transformations (assuming $\mu \geq 0$)

$$U_\pm^{(2)}(t; \mu) = e^{-\gamma t} \psi_\pm \left(\sqrt{2\mu v_0} t \right) \quad (\text{A9})$$

that bring the pair of differential equations (A5) and (A6) into a more recognisable form. We find that $\psi_\pm(z)$ satisfy the following differential equations

$$\frac{d^2\psi_+(z)}{dz^2} + \left(-\frac{\gamma^2}{2\mu v_0} + \frac{1}{2} - \frac{z^2}{4} \right) \psi_+(z) = 0 \quad (\text{A10})$$

$$\frac{d^2\psi_-(z)}{dz^2} + \left(-\frac{\gamma^2}{2\mu v_0} - \frac{1}{2} - \frac{z^2}{4} \right) \psi_-(z) = 0. \quad (\text{A11})$$

These equations resemble the Schrödinger equations for a harmonic oscillator potential. Indeed, the differential equation

$$\frac{d^2f}{dz^2} + \left(p + \frac{1}{2} - \frac{z^2}{4} \right) f(z) = 0 \quad (\text{A12})$$

has two linearly independent solutions $D_p(z)$ and $D_p(-z)$ known as parabolic cylinder functions [45]. Hence, identifying $p = -\gamma^2/(2\mu v_0) = -q$ we can write the most general solutions for $U_\pm^{(2)}(t; \mu)$ as follows.

For $U_+^{(2)}(t; \mu)$ we get

$$U_+^{(2)}(t; \mu) = e^{-\gamma t} \left[A_1(q) D_{-q} \left(\sqrt{2\mu v_0} t \right) + A_2(q) D_{-q} \left(-\sqrt{2\mu v_0} t \right) \right]; \quad \text{with } q = \frac{\gamma^2}{2\mu v_0} \geq 0, \quad (\text{A13})$$

where $A_1(q)$ and $A_2(q)$ are two arbitrary constants to be fixed from the initial conditions in (A7). The two initial conditions $U_+^{(2)}(0; \mu) = 1/2$ and $\dot{U}_+^{(2)}(t=0; \mu) = 0$ give two relations between $A_1(q)$ and $A_2(q)$

$$A_1(q) + A_2(q) = \frac{1}{2 D_{-q}(0)} \quad (\text{A14})$$

$$A_1(q) - A_2(q) = \frac{\gamma}{2\sqrt{2\mu v_0} D'_{-q}(0)}, \quad (\text{A15})$$

where $D'_{-q}(z) = dD_{-q}(z)/dz|_{z=0}$. These two relations fix the two constants

$$A_1(q) = \frac{1}{4} \left(\frac{1}{D_{-q}(0)} + \frac{\gamma}{\sqrt{2\mu v_0} D'_{-q}(0)} \right) = \frac{2^{q/2}}{4\sqrt{\pi}} \left[\Gamma((1+q)/2) - \sqrt{\frac{q}{2}} \Gamma(q/2) \right] \quad (\text{A16})$$

$$A_2(q) = \frac{1}{4} \left(\frac{1}{D_{-q}(0)} - \frac{\gamma}{\sqrt{2\mu v_0} D'_{-q}(0)} \right) = \frac{2^{q/2}}{4\sqrt{\pi}} \left[\Gamma((1+q)/2) + \sqrt{\frac{q}{2}} \Gamma(q/2) \right]. \quad (\text{A17})$$

where we used the explicit values of $D_{-q}(0)$ and $D'_{-q}(0)$ [45].

Similarly, we can find the solution for $U_-^{(2)}(t; \mu)$ (again for $\mu \geq 0$)

$$U_-^{(2)}(t; \mu) = e^{-\gamma t} \left[B_1(q) D_{-q-1} \left(\sqrt{2\mu v_0} t \right) + B_2(q) D_{-q-1} \left(-\sqrt{2\mu v_0} t \right) \right]; \quad \text{with } q = \frac{\gamma^2}{2\mu v_0} \geq 0, \quad (\text{A18})$$

where the two constants $B_1(q)$ and $B_2(q)$ are given by

$$B_1(q) = \frac{1}{4} \left(\frac{1}{D_{-q-1}(0)} + \frac{\gamma}{\sqrt{2\mu v_0} D'_{-q-1}(0)} \right) = -\sqrt{q} \frac{2^{q/2}}{4\sqrt{\pi}} \left[\Gamma((1+q)/2) - \sqrt{\frac{q}{2}} \Gamma(q/2) \right] = -\sqrt{q} A_1(q) \quad (\text{A19})$$

$$B_2(q) = \frac{1}{4} \left(\frac{1}{D_{-q-1}(0)} - \frac{\gamma}{\sqrt{2\mu v_0} D'_{-q-1}(0)} \right) = \sqrt{q} \frac{2^{q/2}}{4\sqrt{\pi}} \left[\Gamma((1+q)/2) + \sqrt{\frac{q}{2}} \Gamma(q/2) \right] = \sqrt{q} A_2(q). \quad (\text{A20})$$

Indeed, by replacing $q \rightarrow -q$, one can now verify explicitly that the symmetry relation in (A8) is satisfied by these solutions $U_{\pm}^{(2)}(t; \mu)$.

Finally, the total cumulant generating function for any μ is given by the sum

$$\begin{aligned} U^{(2)}(t; \mu) &= U_+^{(2)}(t; \mu) + U_-^{(2)}(t; \mu) = \int_{-\infty}^{\infty} e^{-\mu x} p_2(x, t) dx \\ &= e^{-\gamma t} \left[A_1(q) D_{-q} \left(\frac{\gamma}{\sqrt{q}} t \right) + A_2(q) D_{-q} \left(-\frac{\gamma}{\sqrt{q}} t \right) - \sqrt{q} A_1(q) D_{-q-1} \left(\frac{\gamma}{\sqrt{q}} t \right) + \sqrt{q} A_2(q) D_{-q-1} \left(-\frac{\gamma}{\sqrt{q}} t \right) \right] \end{aligned} \quad (\text{A21})$$

where $q = \gamma^2/(2\mu v_0)$ and the two constants $A_1(q)$ and $A_2(q)$ are given respectively in (A16) and (A17). Manifestly, we have the symmetry $U^{(2)}(t; \mu) = U^{(2)}(t; -\mu)$.

We now show briefly how to recover the large deviation behaviour at late times in (76) for $n = 2$ from the exact solution in (A21). To proceed, we first rewrite the exact solution (A21) in terms of $w = \mu v_0 t/(2\gamma)$, i.e., replace $t = 2\gamma w/(\mu v_0)$ and use $q = \gamma^2/(2\mu v_0)$. This gives

$$U(t; \mu) = e^{-\gamma t} [A_1(q) D_{-q}(4\sqrt{q}w) + A_2(q) D_{-q}(-4\sqrt{q}w) - \sqrt{q} A_1(q) D_{-q-1}(4\sqrt{q}w) + \sqrt{q} A_2(q) D_{-q-1}(-4\sqrt{q}w)]. \quad (\text{A22})$$

We will henceforth assume that $\mu > 0$, i.e., $q > 0$ and $w > 0$. For $\mu < 0$, the result will follow from the symmetry $U^{(2)}(t; \mu) = U^{(2)}(t; -\mu)$, which also indicates the symmetry $H_2(w) = H_2(-w)$.

Since $q = \gamma^2/(2\mu v_0) \rightarrow \infty$ as $\mu \rightarrow 0$, we need to analyse (A22) in the limit $q \rightarrow \infty$ keeping w fixed. To take this tricky limit where both the index and the argument of the parabolic cylinder function diverge, we found it convenient to use the following integral representation of $D_{-q}(z)$ [45], valid for $q > 0$

$$D_{-q}(z) = \frac{e^{-z^2/4}}{\Gamma(q)} \int_0^{\infty} e^{-xz - x^2/2 + (q-1) \ln x} dx. \quad (\text{A23})$$

Using this representation, we now evaluate each of the four terms on the right hand side (r.h.s) of (A22) in the $q \rightarrow \infty$ limit. For instance, the first term (excluding the global $e^{-\gamma t}$ factor) can be written as

$$A_1(q) D_{-q}(4\sqrt{q}w) = \frac{A_1(q)}{\Gamma(q)} e^{-4qw^2} \int_0^{\infty} e^{-4\sqrt{q}xw - x^2/2 + (q-1) \ln x} dx, \quad (\text{A24})$$

where $A_1(q)$ is given in (A16). In the large q limit, the integral can be evaluated by the saddle point method. Using also the asymptotic expansion of $\Gamma(q)$ for large q , we find, up to pre-exponential factors

$$A_1(q) D_{-q}(4\sqrt{q}w) \sim e^{q f_1(w)}; \quad \text{where} \quad f_1(w) = -2w \sqrt{1+4w^2} + \ln(\sqrt{1+4w^2} - 2w). \quad (\text{A25})$$

Similarly, the second term gives in the large q limit

$$A_2(q) D_{-q}(-4\sqrt{q}w) \sim e^{q f_2(w)}; \quad \text{where} \quad f_2(w) = 2w \sqrt{1+4w^2} + \ln(\sqrt{1+4w^2} + 2w). \quad (\text{A26})$$

Likewise, one can show that the third term scales as $\sim e^{q f_1(w)}$, while the fourth term scales as $\sim e^{q f_2(w)}$. Now, it is easy to see that for all $w > 0$ (we recall that $w = \mu v_0 t/(2\gamma) > 0$ for $\mu > 0$), $f_2(w) > f_1(w)$. Hence, for large q and $w > 0$, the r.h.s of (A22) scales as

$$U(t; \mu) \sim e^{-\gamma t} e^{q f_2(w)} \sim e^{-\gamma t \left(1 - \frac{f_2(w)}{4w}\right)} \quad (\text{A27})$$

where we replaced $q = \gamma t/(4w)$. From (A27) we read off $H_2(w)$ for $w > 0$

$$H_2(w) = 1 - \frac{f_2(w)}{w} = 1 - \frac{1}{2} \sqrt{1+4w^2} - \frac{1}{4w} \ln(\sqrt{1+4w^2} + 2w); \quad \text{for } w \geq 0. \quad (\text{A28})$$

Note that the result for $H_2(w)$ with $w < 0$ just follows from the symmetry $H_2(-w) = H_2(w)$. In fact, the function $H_2(w)$ in (A28) can be written in a manifestly symmetric form that is valid for all $-\infty < w < \infty$ as

$$H_2(w) = 1 - \frac{1}{2} \sqrt{1+4w^2} - \frac{\text{arcsinh}(2w)}{4w}; \quad -\infty < w < \infty. \quad (\text{A29})$$

This result coincides exactly with (90) derived in Section VI.

3. The case $n = 1/2$

In this case, we start from (63) which for $n = 1/2$ reads

$$\frac{d^2 U^{(1/2)}}{dt^2} + \left(2\gamma + \frac{1}{2t}\right) \frac{dU^{(1/2)}}{dt} - \frac{\mu^2 v_0^2}{\pi t} U^{(1/2)} = 0 \quad (\text{A30})$$

to be solved with the initial conditions in (65). To reduce it to a familiar differential equation we make the following transformation

$$U^{(1/2)}(t; \mu) = \sqrt{2\gamma t} e^{-2\gamma t} F(2\gamma t). \quad (\text{A31})$$

Substituting (A31) in (A30), one can check that $F(z)$ satisfies the differential equation

$$z F''(z) + \left(\frac{3}{2} - z\right) F'(z) - \left(1 + \frac{\mu^2 v_0^2}{2\pi\gamma}\right) F(z) = 0. \quad (\text{A32})$$

This is now of the standard form of the confluent hypergeometric differential equation [44]: $F''(z) + (b - z)F'(z) - aF(z) = 0$, whose general solution is given by a linear combination of two independent confluent hypergeometric functions $U(a, b, z)$ and ${}_1F_1(a, b, z)$. Hence,

$$F(z) = C_1 U\left(1 + \frac{\mu^2 v_0^2}{2\pi\gamma}, \frac{3}{2}, z\right) + C_2 {}_1F_1\left(1 + \frac{\mu^2 v_0^2}{2\pi\gamma}, \frac{3}{2}, z\right), \quad (\text{A33})$$

where C_1 and C_2 are unknown constants. Hence, the general solution of (A30) can be written as

$$U^{(1/2)}(t; \mu) = \sqrt{2\gamma t} e^{-2\gamma t} \left[C_1 U\left(1 + \frac{\mu^2 v_0^2}{2\pi\gamma}, \frac{3}{2}, 2\gamma t\right) + C_2 {}_1F_1\left(1 + \frac{\mu^2 v_0^2}{2\pi\gamma}, \frac{3}{2}, 2\gamma t\right) \right]. \quad (\text{A34})$$

The unknown constants are fixed from the initial conditions in (65). This gives

$$C_1 = \frac{\Gamma\left(1 + \frac{\mu^2 v_0^2}{2\pi\gamma}\right)}{\sqrt{\pi}}; \quad \text{and} \quad C_2 = 2 \frac{\Gamma\left(1 + \frac{\mu^2 v_0^2}{2\pi\gamma}\right)}{\Gamma\left(\frac{1}{2} + \frac{\mu^2 v_0^2}{2\pi\gamma}\right)}. \quad (\text{A35})$$

Hence the final exact cumulant generating function for $n = 1/2$ is given by

$$U^{(1/2)}(t; \mu) = \sqrt{2\gamma t} e^{-2\gamma t} \Gamma\left(1 + \frac{\mu^2 v_0^2}{2\pi\gamma}\right) \left[\frac{1}{\sqrt{\pi}} U\left(1 + \frac{\mu^2 v_0^2}{2\pi\gamma}, \frac{3}{2}, 2\gamma t\right) + \frac{2}{\Gamma\left(\frac{1}{2} + \frac{\mu^2 v_0^2}{2\pi\gamma}\right)} {}_1F_1\left(1 + \frac{\mu^2 v_0^2}{2\pi\gamma}, \frac{3}{2}, 2\gamma t\right) \right]. \quad (\text{A36})$$

In the limit $t \rightarrow \infty$, $\mu \rightarrow \infty$ but keeping $w = 2\mu v_0/\gamma\sqrt{\pi t}$ fixed, we expect that this exact solution should converge to the large deviation form

$$U^{(1/2)}(t; \mu) \sim \exp\left[-\gamma t H_{1/2}\left(w = \frac{2\mu v_0}{\gamma\sqrt{\pi t}}\right)\right], \quad (\text{A37})$$

where the rate function $H_{1/2}(w)$ is given in (102). We have not proved it here, but we have checked by Mathematica that indeed the exact solution (A36) does converge to this expected large deviation form in (A37).

-
- [1] S. N. Majumdar, C. Sire, A.J. Bray and S. J. Cornell, **77**, 2867 (1996).
[2] A. J. Bray, S. N. Majumdar, and G. Schehr, *Adv. in Phys.* **62**, 225 (2013).
[3] M. C. Wang and G. E. Uhlenbeck, *Rev. Mod. Phys.* **17**, 323 (1945).
[4] A. Lachal, *The Ann. of Prob.* **25**, 1712 (1997).
[5] S. J. Cornell, M. R. Swift, and A. J. Bray, *Phys. Rev. Lett.* **81**, 1142 (1998); M. R. Swift and A. J. Bray, *Phys. Rev. E* **59**, R4721 (1999); T. W. Burkhardt, J. Franklin, and R. R. Gawronski, *Phys. Rev. E* **61**, 2376 (2000).
[6] S. N. Majumdar and A. J. Bray, *Phys. Rev. Lett.* **86**, 3700 (2001).

- [7] H. Kleinert, *J. Math. Phys.* **27**, 3003 (1986).
- [8] T. W. Burkhardt, *J. Phys. A* **26**, L1157 (1993).
- [9] D. S. Dean, B. Miao, and R. Podgornik, *J. Phys. A: Math. Theor.* **52**, 505003 (2019).
- [10] G.J. Papadopoulos, *J. Phys. A* **1**, 431 (1968); G.J. Papadopoulos and J. Thomchick, *J. Phys. A: Math. Gen.* **10**, 1115 (1977).
- [11] D.A. Smith, *J. Phys. A* **34**, 4507 (2001).
- [12] D. Kachan, R. Bruinsma and A. J. Levine, *Phys. Rev. E* **87**, 032719 (2013).
- [13] N. Uchida, *Phys. Rev. Lett.* **87**, 216101 (2001).
- [14] D. S. Dean, B. Miao, and R. Podgornik, to appear in *J. Phys. A: Math. Theor.* (2020).
- [15] J.Z. Simon, *Phys. Rev. D* **41**, 3720 (1990).
- [16] Y. G. Sinai, *Theor. Math. Phys.* **90**, 219 (1992).
- [17] T. W. Burkhardt, in *First-Passage Phenomena and Their Applications*, ed. R. Metzler, G. Oshanin, and S. Redner (World Scientific, 2014).
- [18] S. N. Majumdar, *Curr. Sci.* **77**, 370 (1999).
- [19] G. Schehr and S. N. Majumdar, *Phys. Rev. Lett.* **99**, 060603 (2007).
- [20] M. Poplasvskyi and G. Schehr, *Phys. Rev. Lett.* **121**, 150601 (2018).
- [21] M. Kac, *Rocky Mountain J. Math.* **4**, 497 (1974).
- [22] J. Masoliver and G. H. Weiss, *Eur. J. Phys.* **17** 190 (1996).
- [23] G.H. Weiss, *Physica A*, **311**, 381 (2002).
- [24] J. Masoliver and K. Lindenberg, *Eur. Phys. J B* **90**, 107 (2017).
- [25] H. C. Berg, *E. coli in Motion* (Springer, 2014).
- [26] J. Tailleur and M. E. Cates, *Phys. Rev. Lett.* **100**, 218103 (2008).
- [27] S. Herrmann and P. Vallois, *Stoch. Dyn.* **10**, 161 (2010).
- [28] H. G. Othmer, S. R. Dunbar, and W. Alt, *J. Math. Biol.* **26**, 263 (1988).
- [29] K. Martens, L. Angelani, R. Di Leonardo, and L. Bocquet, *Eur. Phys. J E* **35**, 84 (2012).
- [30] K. Malakar et. al., *J. Stat. Mech.* 043215 (2018).
- [31] M. R. Evans and S. N. Majumdar, *J. Phys. A: Math. Theor.* **51**, 475003 (2018).
- [32] A. Dhar, A. Kundu, S. N. Majumdar, S. Sabhapandit and G. Schehr, *Phys. Rev. E*, **99**, 032132 (2019).
- [33] I. Santra, U. Basu, and S. Sabhapandit, *Phys. Rev. E* **101**, 062120 (2020).
- [34] L. Angelani, R. Di Leonardo, and M. Paoluzzi, *Eur. Phys. J. E* **37**, 59 (2014).
- [35] L. Angelani, *J. Phys. A: Math. Theor.* **48**, 495003 (2015).
- [36] P. Le Doussal, S. N. Majumdar, and G. Schehr, *Phys. Rev. E* **100**, 012113 (2019).
- [37] P. Singh and A. Kundu, *J. Stat. Mech.* 083205 (2019).
- [38] P. Le Doussal, S. N. Majumdar, and G. Schehr, *Europhys. Lett.* **130**, 40002 (2020).
- [39] T. Banerjee, S. N. Majumdar, A. Rosso, and G. Schehr, *Phys. Rev. E* **101**, 052101 (2020).
- [40] F. Mori, P. Le Doussal, S. N. Majumdar, and G. Schehr, *Phys. Rev. Lett.* **124**, 090603 (2020).
- [41] A. J. Bray, *Adv. Phys.* **43**, 357 (1994).
- [42] D. Osmanović and Y. Rabin, *Soft Matter* **13**, 963 (2017); D. Osmanović, *J. Chem. Phys.* **149**, 164911 (2018).
- [43] S. Chaki and R. Chakrabarti, *J. Chem. Phys.* **150**, 094902 (2019).
- [44] M. Abramowitz and I. A. Stegun, *Handbook of Mathematical Tables*, (Dover, New York, 1965).
- [45] I S Gradshteyn and I M Ryzhik, *Tables of Integrals, Series, and Products* (New York: Academic, 1980).
- [46] S. N. Majumdar, *Curr. Sci.*, **89**, 2076 (2005).
- [47] W. K. Hastings, *Biometrika* **57**, 97 (1970)
- [48] N. Metropolis, A. W. Rosenbluth, M. N. Rosenbluth, A. H. Teller, and E. Teller, *J. Chem. Phys.* **21**, 1087 (1953).
- [49] A. K. Hartmann, *Eur. Phys. J. B* **84**, 627 (2011), ISSN 1434-6036.
- [50] M. Newman and G. Barkema, *Monte carlo methods in statistical physics chapter 1-4* (Oxford University Press: New York, USA, 1999).
- [51] H. Schawe, A. K. Hartmann, and S. N. Majumdar, *Phys. Rev. E* **97**, 062159 (2018).
- [52] A. K. Hartmann and M. Mézard, *Phys. Rev. E* **97**, 032128 (2018).
- [53] H. Schawe, A. K. Hartmann, S. N. Majumdar, and G. Schehr, *EPL (Europhys. Lett.)* **124**, 40005 (2018).
- [54] J. Börjes, H. Schawe, and A. K. Hartmann, *Phys. Rev. E* **99**, 042104 (2019).
- [55] A. K. Hartmann, S. N. Majumdar, H. Schawe, and G. Schehr, *J. Stat. Mech.* **2020**, 053401 (2020).
- [56] H. Schawe, A. K. Hartmann, and S. N. Majumdar, *Phys. Rev. E* **96**, 062101 (2017).
- [57] H. Schawe and A. K. Hartmann, *Euro. Phys. J. B* **92**, 73 (2019), ISSN 1434-6036.